Effects of Lithographic Parameters and Geometric Exposure Method for Corner Rounding Correction in Massively-Parallel Electron-Beam Systems for the Mask Pattern Development

by

Soomin Moon

A thesis submitted to the Graduate Faculty of
Auburn University
in partial fulfillment of the
requirements for the Degree of
Master of Science

Auburn, Alabama
August 8, 2020

Keywords: Critical dimension, Dose latitude, Electron beam lithography, Exposure variation, Exposure contrast, Line edge roughness, Corner rounding, Directivity, Geometric proximity correction, Mask development, Massively-parallel beams

Approved by

Mark L. Adams, Chair, Associate Professor of Electrical and Computer Engineering
Michael C. Hamilton, Professor of Electrical and Computer Engineering
Lloyd Riggs, Professor of Electrical and Computer Engineering

Abstract

The ability of electron-beam (e-beam) lithography to transfer fine features onto a substrate is essential in many applications where high-resolution devices need to be fabricated. However, its low throughput has been the major drawback, especially for transferring large-scale patterns such as optical masks. In order to overcome the drawback, e-beam lithography systems with massively-parallel beams were recently developed and their throughput, improved by several orders of magnitude, has been experimentally demonstrated. In this study, for the optimal use of such parallel-beam systems, the effects of lithographic parameters on the writing quality are analyzed, and the approaches to improve the writing quality of the pattern corner are explored. The metrics of writing quality include the exposure variation and contrast, the total dose required, the dose latitude, the line edge roughness, the corner rounding, and directivity. The proposed correction method analysis including the correction impact from the size of the correction beam, the necessary number of correction beams, correction trade off characteristics from the overlap amount with the regular shot, and design guidelines are discussed. The analysis results obtained through an extensive simulation are provided and discussed in this thesis.

Acknowledgments

This work would not have been possible without the financial support of the Samsung Electronics Co., Ltd and the department of Electrical and Computer Engineering of the Auburn University. I am especially indebted to my thesis advisor, Dr. Mark Adams, who have been supportive of my career goals and who worked actively to provide me with the protected academic time to pursue these goals.

I am grateful to all of those with whom I have had the pleasure to work during this and other related projects. Each of the members of my dissertation committee has provided me extensive personal and professional guidance and taught me a great deal about both academic research and life in general. I would like to pay my special regards to the department chair, Dr. Mark Nelms and the department graduate program officer, Dr. John Hung. Without their support, I would not have considered a graduate study and successfully complete the master's program.

I wish to show my gratitude to the mentors I met during the graduate program. I would especially like to thank Dr. Lloyd Riggs, Dr. Michael Hamilton, Dr. Michael Baginski, Dr. Christopher Harris. I would to like to recognize the invaluable assistance of the researchers of the relevant field. I would like to thank the Auburn University Librarian, Ms.Juliet Rumble. I whole-heartedly respect Dr. Sylvester Johnson IV of Cornell University Physics department for reaching out to me about his dissertation work which dates back to 30 years that he could promptly and a clearly answer my questions.

Also, I want to thank Dr. Yuan Meng for giving me feedback on preparing for my thesis defense. And I would like to thank Major Hyesung Ji from the Korean Ministry of National Defense, John Ragland, and Dehua Li.

Nobody has been more important to me in the pursuit of this project than the members of my family. Lastly, I would like to thank my parents and late dog brother, Darong for endless support.

Table of Contents

List of Figures

List of Tables

Chapter 1

INTRODUCTION

Electron-beam lithography (EBL) has a capability of transferring a fine-feature pattern onto a substrate and is widely used in various applications of pattern transfer.[1–5] However, its main drawback of low throughput has become a limiting factor for large-scale patterns as the pattern size and complexity continue to increase. In response to the need for significant improvement of writing throughput, there have been many efforts to develop EBL systems which utilize multiple beams.[6–10] Some of those efforts recently lead to fruitful outcomes, new EBL systems with massively-parallel beams. While the patterning throughput has been improved by several orders of magnitude,[6,9] there is a need to analyze the writing quality in order to enable the optimal use of such systems. In this study, the dependency of writing quality on lithographic parameters are examined and the geometric proximity correction guidelines to improve the writing quality of the pattern corner are explained.

In a massively-parallel EBL system, each beam can be considered to be a fixed shaped-beam which is dependent on the beam aperture. First, due to the beam blur along the boundary of a beam and electron scattering in the resist,[11] the spatial distribution of exposure (energy deposited in the resist) within a feature may not be uniform even when all points in the feature are exposed with a constant dose. The scattering effect leads to an undesired influence in the region adjacent to those exposed by the electron beam is called the proximity effect.[12] Second, the number of bits used to encode a dose level for each beam may be limited to reduce the required rate of data transfer into the e-beam control unit.[13] As a way to increase the dose resolution, each point (pixel) on the resist surface may be allowed to be exposed by multiple beams in an overlapping manner. That is, the exposing interval can be smaller than the pixel interval (size), which slows the exposure change over the feature boundary. Third, it is possible

that some of beams may become faulty and are not able to provide the specified level of dose to certain pixels. Though the fault rate is typically very low, the effect of faulty beams, i.e., the exposure reduction at a pixel or pixels, may not be negligible.

The above mentioned effects can cause a substantial change in the spatial distribution of exposure and therefore the writing quality. Through an extensive simulation, the writing quality such as exposure variation and contrast, total dose, line edge roughness, maximum indent, dose latitude, and corner rounding is analyzed in terms of the lithographic parameters such as the exposing interval, etc. This study is a first step toward the development of a method to optimally utilize an e-beam system with massively-parallel beams. The results indicate that the effects can be substantial and therefore need to be taken into account.

In massively-parallel EBL system, a significant pattern degradation occurs at the corner of the feature due to a non-uniform dose deposition over the corner pixels after exposure by numerous overlapping beams. Many overlapping beams deposit dose mostly at the center of the feature and the dose level decays to the edge of the feature. The corner rounding is proportional to the amount of overlap exposure of the feature. The writing also inherently suffers at the feature corner even when the feature is patterned without any overlapping beams due to the beam blur along the boundary of the beam. As a first step for proximity correction of the system, the study limits the corner correction for the simplest writing strategy where beams do not overlap and the pixel size equals the beam size. The corner correction of a feature written with overlapping beams is left for future work.

Conventionally, proximity effect is remedied by changing the feature geometries. The proximity correction feature changes the geometry of the feature by adding or subtracting shapes from the desired feature pattern.[14] Often times the proximity corrected pattern is partitioned into different shapes with smaller areas to optimize the correction depending on the complexity of the original pattern.[15,16] If the pattern is a rectangular shape it is simple enough that the proximity correction at the corner does not require a pattern decomposition step. The non-ideal exposure distribution at the corner of the rectangular pattern is typically improved by means of transferring additional beams[17–23] in the vicinity of the feature corner. This method intends to change the shape of the exposure and increase the level of the energy deposited. The

majority of the typical approach patterns a small single square beam that either touches the corner of the feature[17] or partially overlaps with the corner of the feature.[18] Various shapes used for the correction include a rectangle,[19] octagon,[20] etc. Other approaches apply a rotation of the shot's[19–21] orientation by 45° at the corner of the feature. A multiple number of shots has been used to surround the corner of the feature[22,23] using a combination of a rectangular shaped beams and a square beams[22] or exposing a number of identical square beams.[23] Unlike the previous studies, this study explores the plausible approaches allowed given the constraints of the massively parallel e-beam system. Such constraints include non-rotation of the beam, fixed beam size and shape at each operation, and synchronous control of the beams.

Through extensive simulation in this study, the writing quality improvement is explored for the possibility of using multiple identical shape of correction shots in terms of parameters such as varying the size of the correction shot, dose, and the amount of overlap exposure of the correction shot with the regular shot. The study evaluates the correction quality at the corner in respect to the corner rounding area and the directivity coordinates. The guidelines for the correction strategy are based on the development trade offs from the amount of overlap.

In Chapter 2, a model of a massively-parallel EBL system is described. In Chapter 3, the metrics of writing quality are introduced. In Chapter 4, the simulation study is described. In Chapter 5, the results are presented and discussed. In Chapter 6, the proposed strategy is defined and explained, followed by a summary in Chapter 7.

Chapter 2

A Model of Massively-Parallel System

In a massively-parallel system like the eMET,[6–8] a large number of beams are generated through a 2-D array of apertures, each of which defines a beam. The beam size and interval are adjusted by electronic lenses before the beams reach the substrate. While beams can be individually turned on and off, the deflection of beams, which may be needed in a certain writing strategy, is executed in a synchronized manner, i.e., the same deflection angle for all beams. The analysis in this study focuses on the exposure distribution in the resist and its effects on the writing quality. Therefore, the beams arriving at the surface of resist are of interest regardless of the processes of their generation, adjustment and control.

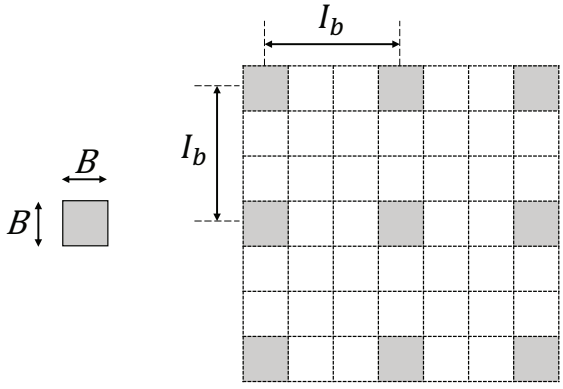

Figure 2.1: Each beam is shaped through a square aperture and the size of beam at the resist surface is $B \times B$. An illustration of beam array is provided where $I_b = 3B$.

In Fig. 2.1, a 2-D array of beams at the surface of resist is illustrated where a square aperture is assumed. The beam size is $B \times B$ and the beam interval is I_b in both dimensions. Normally, I_b is significantly larger than B in a massively-parallel system. In most cases, the spatial variation of exposure within a feature due to the gap between adjacent beams needs to be avoided. A writing strategy may adjust the on-off frequency of beams as the substrate moves

under the parallel beams such that the distance between two adjacent points exposed is less than I_b. The distance between two adjacent exposed points is referred to as the exposing interval, I_e, in both dimensions. The directly exposed regions of size $B \times B$ may overlap depending on B and I_e as shown in Fig. 2.2.

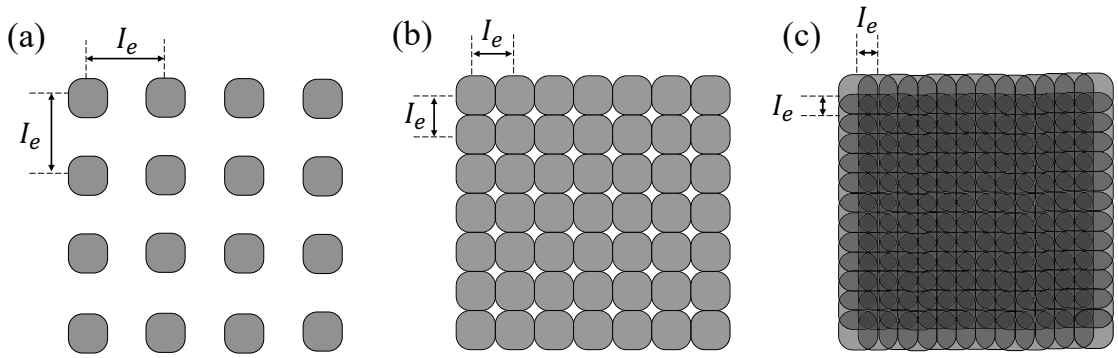

Figure 2.2: Exposing interval I_e varies depending on the writing strategy: (a) $I_e > B$ where $I_e = 2B$, (b) $I_e = B$, and (c) $I_e < B$ where $I_e = B/2$.

Each beam may be considered as a shaped beam where the (cross-section) shape is determined by the aperture and is assumed to be square in this study. The beam blur occurs as a beam goes through the aperture and travels down from the electron source to the resist surface.[11] Electrons also scatter once they contact the resist which further blurs the beam. Therefore, the spatial distribution of exposure contributed by a beam shows a certain degree of blurring over the beam boundary. The spatial distribution of exposure contributed from a shaped beam is referred to as a *transfer function* to be distinguished from a point spread function. The transfer function is modeled to be flat at its center and decreases over its boundary. The decrease follows a Gaussian function such that the peak of the Gaussian function equals the exposure in the flat region and the exposure at the boundary is a half of the peak. The sharpness of the transfer function is controlled by the standard deviation σ of a Gaussian function, which is referred to as the *blurring factor*. An example of a transfer function is shown in Fig. 2.3.

The massively parallel e-beam system can generate different sizes of beams by adjusting the projection system as in Fig. 2.4. According to the beam divergence, a constant energy source can produce a different beam blur which subsequently affects the size of the beam. The sharpness of the beam proportionally increase as the size of the beam decreases. The beams

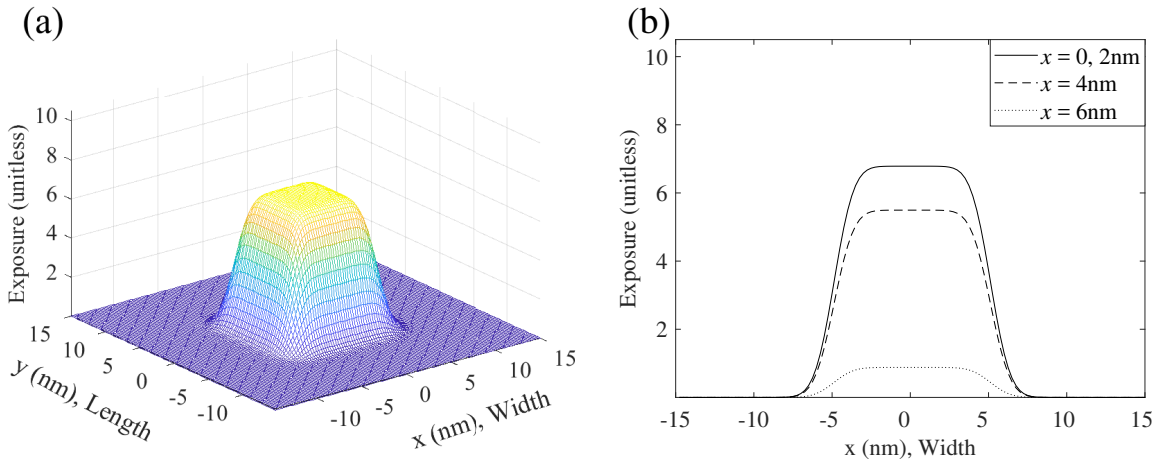

Figure 2.3: (a) 3-D view and (b) cross-section of the transfer function with B = 10 nm and σ = 1 nm.

are generated through the 2-D array of aperture sizes so that different size of beams can not be written parallel. Thus, if a different size of beams are required to pattern a feature, then each beam needs to be patterned during a different run.

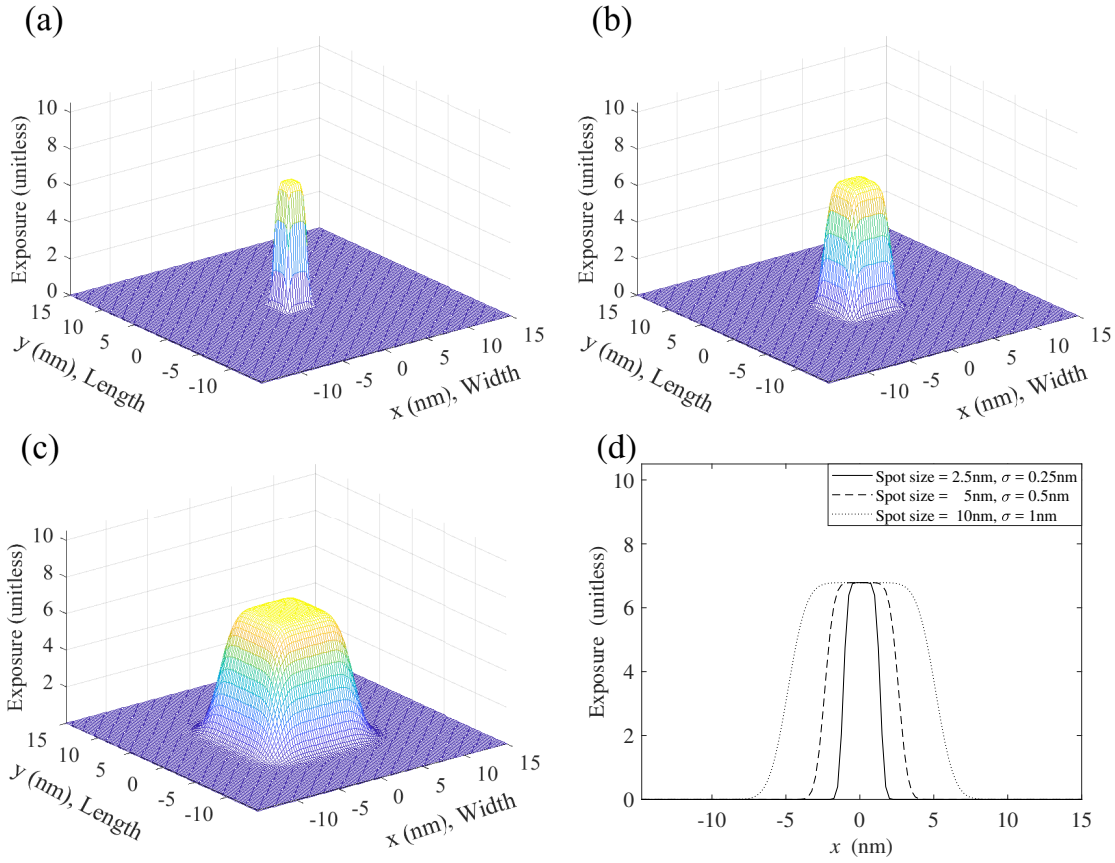

Figure 2.4: (a) 3-D view of the transfer function with B = 2.5 nm and σ = 0.25 nm, (b) with B = 5 nm and σ = 0.5 nm, (c) with B = 10 nm and σ = 1 nm, and (d) cross-section at the center of the transfer function with (a) B = 2.5 nm, (b) 5 nm, and (c) 10 nm.

Chapter 3

Quality Metrics

In analyzing the writing quality, several metrics are considered, i.e., exposure variation within a feature, exposure contrast over the feature boundary, line edge roughness, total dose, dose latitude, corner rounding, directivity, etc. In the analysis, the feature of a single line is considered which is exposed by parallel beams where the dose is constant for all beams. The notations below are adopted in this paper.

B: the dimension of a square regular beam

B_c: the dimension of a square correction beam

x: the width dimension of feature

y: the length dimension of feature

z: the resist-depth dimension

W: the width of a feature

L: the length of a feature

$d(x, y)$: the dose distribution

$e(x, y, z)$: the exposure distribution in the resist

$t(x, y, z)$: the transfer function

$f_a(x, y, z)$: the description of the actual developed pixel in the resist

$f_i(x, y, z)$: the description of the ideal developed pixel in the resist

The 3-D exposure distribution in the resist may be computed through a discrete convolution as in Eq. 3.1,

$$e(x, y, z) = \sum_{x'} \sum_{y'} d(x', y') t(x - x', y - y', z) \tag{3.1}$$

where $d(x, y)$ specifies the spatial distribution of the dose given by all beams.

3.1 Exposure Variation

In general, it is desired that the spatial variation of exposure within each feature is minimal since the variation causes an uneven development of resist and may lead to a rough boundary of the feature. The exposure variation may be quantified as the standard deviation of exposure within a feature at a certain resist layer, z_i.

$$\sigma_e = \sqrt{\frac{1}{WL}\sum_{y=0}^{L}\sum_{x=0}^{W}(e(x, y, z_i) - \overline{e}(x, y, z_i))^2} \tag{3.2}$$

where $\overline{e}(x, y, z_i) = \frac{1}{WL}\sum_{y=0}^{L}\sum_{x=0}^{W} e(x, y, z_i)$.

Such quantification can be dominated by the exposure drop over the boundary of a feature, especially when the drop occurs over a significant distance as shown in Fig. 3.1. Therefore, another measure of exposure variation may be considered, which excludes the exposure drop over the feature boundary, shown as exposure fluctuation in Fig. 3.1. The exposure variation is analyzed in this study.

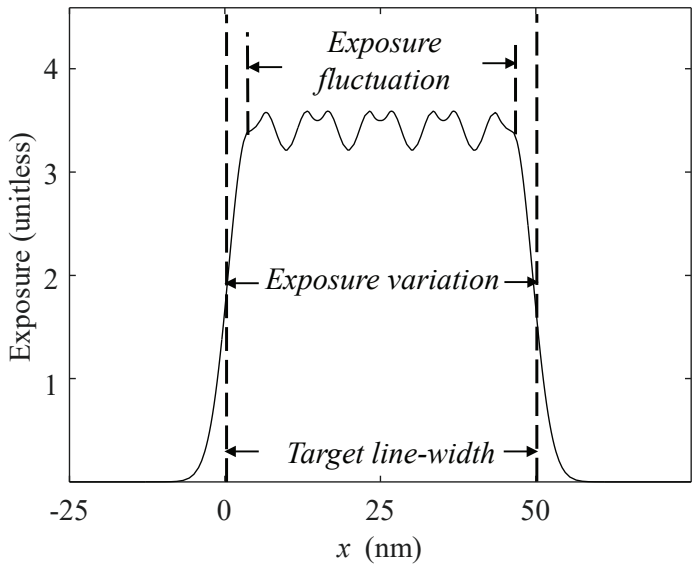

Figure 3.1: Exposure variation is computed within the target line-width and the exposure fluctuation refers to the exposure variation excluding the large change of exposure over the feature edges. I_e = B = 10 nm, W = 50 nm, and σ = 3 nm.

3.2 Exposure Contrast

When a feature is exposed with a uniform dose, the exposure is high in the interior region of the feature and decreases toward and over the feature boundary. The exposure contrast is typically defined as the exposure change over the feature boundary. The exposure may fluctuate spatially and, therefore, the exposure contrast is defined as the difference between the exposure averages over multiple points inside and outside a feature as in Eq. 3.3.

$$C_e = \frac{1}{n_c L} \sum_{y=0}^{L} \left(\sum_{x=0}^{n_c-1} e(x, y, z_i) - \sum_{x=-n_c}^{-1} e(x, y, z_i) \right) \tag{3.3}$$

where n_c is the number of points over which the exposure average is computed ($n_c = 4$ in Fig.3.2) and $x = 0$ corresponds to the feature boundary.

A higher the exposure contrast produces a more stable feature boundary during the development process. The main factor affecting the exposure contrast is the shape of transfer function. Given a transfer function, the exposing interval I_e, e.g., overlapping between the domains of beams, can also affect the exposure contrast as illustrated in Fig. 3.2.

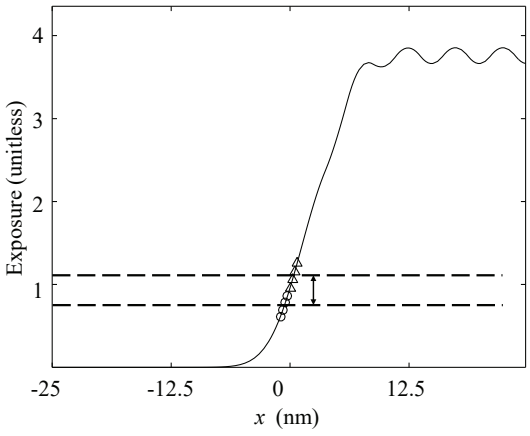

Figure 3.2: Exposure contrast is computed as the difference of the exposure averages evaluated at multiple points inside and outside a feature. In this illustration, x = 0 corresponds to the feature edge and the exposures at four points each inside (triangle) and outside (circle) are involved. B = 10 nm, I_e = 5 nm, W = 50 nm, and σ = 3 nm.

3.3 Total Dose

A higher dose usually makes a larger area of resist develop for a given developing time. However, it is possible that two different doses may lead to the same size of feature after the development, depending on the exposure distribution. From the viewpoint of reducing the writing time, a lower total dose would be preferred. Hence, the total dose, D_t, required for a unit-length segment of a line to develop to the target line-width is considered in this study. Then, it can be shown that D_t is derived as in Eq. 3.4.

$$D_t = \frac{d}{I_e}\left(\frac{W-B}{I_e}+1\right) \tag{3.4}$$

where d is the dose per beam required to achieve the target line-width.

3.4 Line Edge Roughness

The roughness of feature boundary is mainly caused by the stochastic exposure fluctuation and developing process. Another possible source of boundary roughness is the systematic variation in the spatial distribution of the exposure, caused by the shape of transfer function and exposing interval. Also, faulty beams may introduce localized drops in the spatial distribution of the exposure, which can contribute to the roughness. In this study, the line edge roughness (LER) due to the systematic exposure variation and faulty beams is analyzed. The LER is quantified as the standard deviation of edge location in a line feature, which can be expressed as follows:

$$LER = \sqrt{\frac{1}{L}\sum_{y=0}^{L}(x_e(y)-\overline{x}_e)^2} \tag{3.5}$$

where $x_e(y)$ is the edge location and $\overline{x}_e$ is the average edge location, i.e. $\overline{x}_e = \frac{1}{L}\sum_{y=0}^{L} x_e(y)$.

Along with the LER, the maximum indent (see Fig. 3.3) is also a meaningful metric, which can cause a bottle-neck increasing the resistance of a signal path. The maximum indent is measured as the distance from the average edge location to the farthest edge point inward. That is, the maximum indent $(\Delta x_e)_{max}$ can be represented as:

$$(\Delta x_e)_{max} = \max_y(\mid x_e(y) - \overline{x}_e \mid) \tag{3.6}$$

It needs to be pointed out that the LER and maximum indent considered in this study do not include the boundary roughness caused by the randomness in the exposure and developing processes. Only the boundary roughness due to the periodic variation of exposure determined by the transfer function and lithographic parameters is considered, i.e., the roughness one may get even when the exposing and developing processes are deterministic.

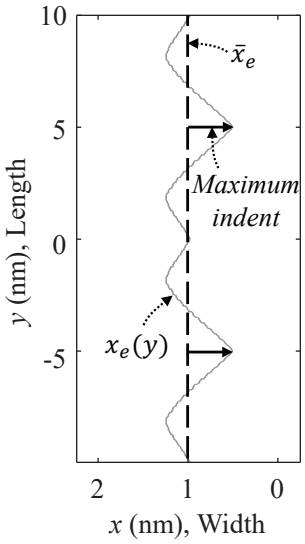

Figure 3.3: LER is computed as the standard deviation of edge location $x_e(y)$ (solid) and the maximum indent is the largest distance inward to the edge from the average edge location $\overline{x}_e$ (dashed). In this illustration, the left boundary of a line feature is shown. B = 10 nm, I_e = 10 nm, W = 30 nm, and σ = 3 nm.

3.5 Dose Latitude

As the dose level varies, the critical dimension (CD), e.g., line-width, of a feature changes. The sensitivity of CD to the dose level is referred to as dose latitude which may be defined as the dose variation causing the +/- 2% variation of CD. Given a substrate system and a developing process, the dose latitude is mainly determined by the spatial distribution of exposure, which in turn depends on the lithographic parameters.

The dose latitude is computed as follows:

$$dose\ latitude = \frac{d_{102} - d_{98}}{d_{100}} \times 100\% \tag{3.7}$$

where d_{98}, d_{100}, and d_{102} are the doses required to develop to the 98%, 100% and 102% of the target CD, respectively.

3.6 Corner Rounding

The corner rounding is mainly caused by the non-ideal exposure distribution from the shape of the transfer function. Given a transfer function, the exposing interval I_e can contribute to the corner rounding as well. Also due to its spatial location, the exposure level at the corner of the feature is lower than the exposure level at the edge of the feature because there is no contribution from neighboring beams. Fig. 3.4 illustrates one quarter of the feature after it is developed and identifies its ideal boundary. The curvature of the developed corner fits one quarter of a circle. And the ideal boundary is tangent to both the rounded feature corner and the edges of the actually developed feature. Then the corner of the ideally developed feature forms a 90° angle as shown in Fig. 3.5(a).

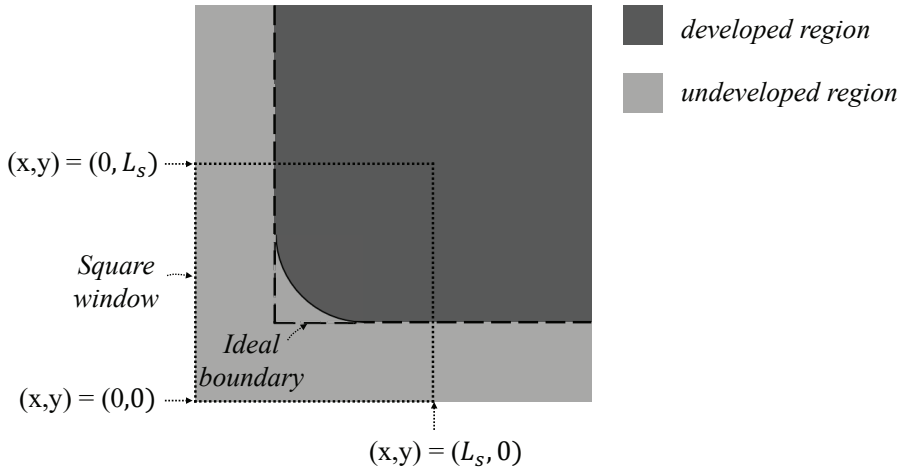

Figure 3.4: Corner rounding is computed as the sum of the number of pixels between the actual developed feature boundary and the ideal developed boundary. In this illustration, a quarter piece of the feature is shown.

The pixel from an ideal development can be expressed by $f_i(x, y, z_i)$ as below.

$$f_i(x, y, z_i) = \begin{cases} 1, & \text{if the pixel } (x, y, z_i) \text{ is a developed pixel from an ideal development.} \\ 0, & \text{otherwise.} \end{cases} \tag{3.8}$$

The Fig. 3.5(b) describes the pixel from an actual development which can be expressed by $f_a(x, y, z_i)$ as below.

$$f_a(x, y, z_i) = \begin{cases} 1, & \text{if the pixel } (x, y, z_i) \text{ is a developed pixel from an actual development.} \\ 0, & \text{otherwise.} \end{cases} \tag{3.9}$$

The corner rounding is defined as the amount of area between the actual developed feature boundary and the ideal developed boundary. The corner rounding is quantified as the sum of the number of pixels deviated from the ideal developed boundary which is computed within a square window of L_s. The size of the square window is set large enough that it could include any deviated pixels outside of the developed edge of the feature. The corner rounding is expressed as follows:

$$Corner\ rounding = \sum_{y=0}^{L_s} \sum_{x=0}^{L_s} (|\ f_a(x, y, z_i) - f_i(x, y, z_i)\ |) \tag{3.10}$$

where the absolute difference of $f_a(x, y, z_i)$ from $f_u(x, y, z_i)$ is illustrated in Fig. 3.5(c).

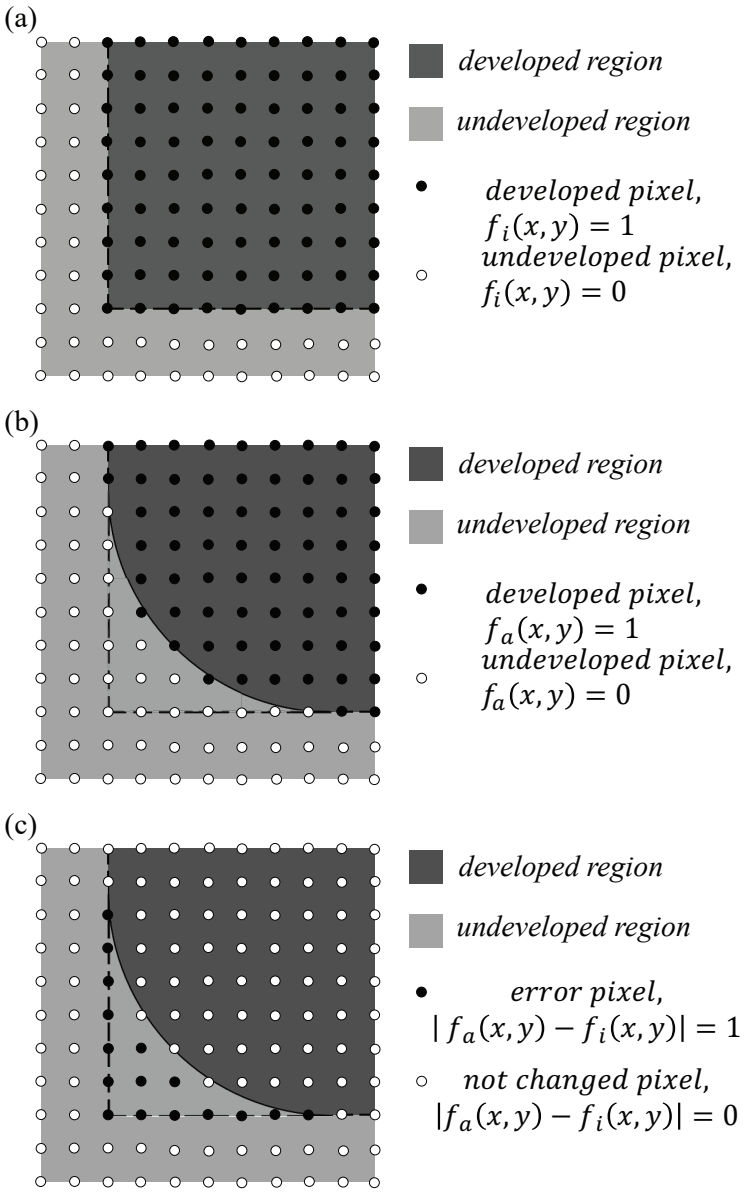

Figure 3.5: An illustration of (a) ideal developed feature using pixel representation in $f_i(x, y)$, (b) actual developed feature using pixel representation in $f_a(x, y)$, and (c) corner rounding which indicates the pixel of deviation in $|\ f_a(x, y, z_i) - f_i(x, y, z_i)\ |$.

3.7 Directivity

When a correction shot is patterned, the corner rounding is reduced and the resulting corner of the feature gets closer to the ideal corner of the feature. The directivity indicates the quality of development at the corner on how close it achieves an ideal corner shape. Directivity is dependent on the size of the correction shot. Larger shots are more directive than smaller shots because they are able to generate a more ideal corner pattern when the overlap of both size of shots is held constant. The directivity is defined as the (x,y) coordinates of developed edge point at the corner of the feature. It is measured along the y = x, a diagonal line that divides the square regular shot at the corner of the feature exactly in half as in the green line in Fig. 3.6. The effect of correction is recognized visually by the (x,y) coordinates using arrows on the contour of the developed boundary of the feature at each layer. In Fig. 3.6, the blue arrow represents the (x,y) coordinates before the correction, and the red arrow represents the (x,y) coordinates after the correction. If the red arrow is closer to the ideal feature corner in the figure and away from the blue arrow, then the correction shot is more directive.

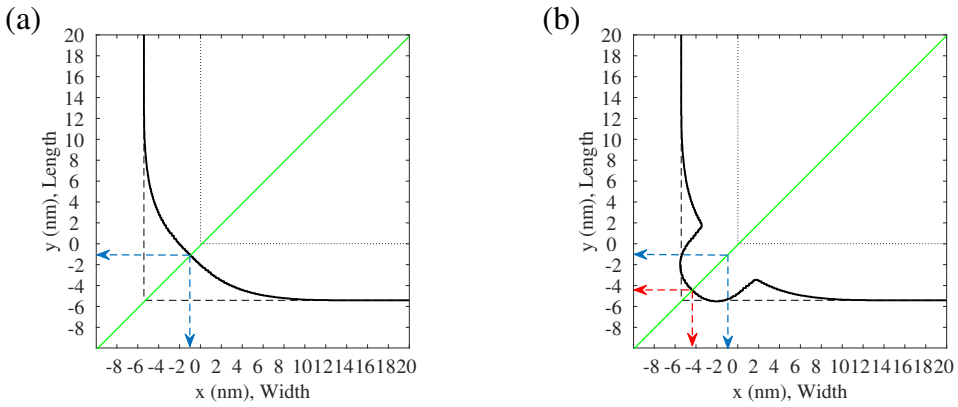

Figure 3.6: The directivity is defined as a (x,y) coordinates of developed edge point at the corner of the feature at each layer which is measured along the y = x, the diagonal line in green: (a) before correction (x,y) = (-1 nm,-1 nm) and (b) after correction (x,y) = (-4 nm,-4 nm). The blue arrow represents the corner (x,y) coordinates before the correction and the red arrow represents the corner (x,y) coordinates after the correction.

Chapter 4

Simulation

A single line is exposed by a massively-parallel e-beam system along its length dimension on a typical substrate. The 3-D exposure distribution in the resist is computed at the resolution, I_s, referred to as the *simulation interval* where $I_s < I_e$ to be able to consider the detail of exposure distribution as shown in Fig. 4.1. In this study, I_s is set to $\frac{I_e}{4}$. The resist is modeled by 5 layers to take into account the layer dependency of exposure and at the same time avoid additional computational complexity. From the exposure distribution, the exposure variation and contrast are computed. The developing-rate distribution is derived from the exposure distribution and then the remaining resist profile is obtained through a resist-development simulation.[24] The development simulation continues until the line feature is fully developed to the bottom layer of resist. From the resist profile, the maximum indent, LER, and corner rounding are quantified. The total dose required and dose latitude can be found by repeating the development simulation.

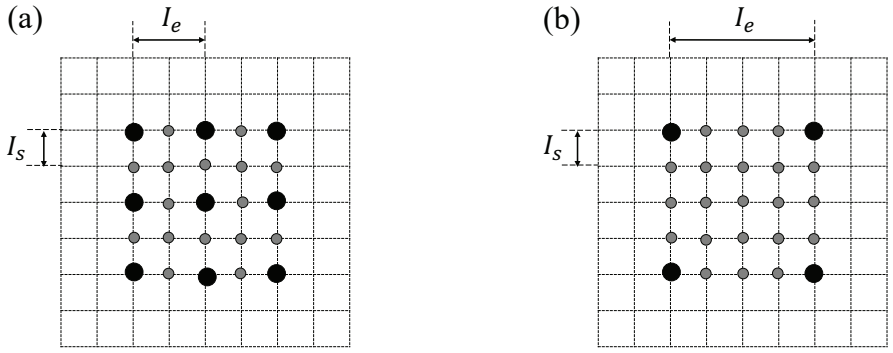

Figure 4.1: In the simulation, the exposure is evaluated at a finer resolution (I_s) than the exposing interval (I_e): (a) $I_s = \frac{I_e}{2}$ and (b) $I_s = \frac{I_e}{4}$. The dark points are exposed and the exposure is computed at both dark and gray points.

The aperture is assumed to be a square as in the currently available systems, and the beam cross-section at the surface of resist is 10 nm $\times$ 10 nm (B = 10 nm). The exposing interval is varied from 1 nm to 10 nm and the blurring factor of transfer function is varied from 1 nm to 4 nm. The simulation interval is 0.25 nm. The line feature is 150 nm long and the middle 60% segment is used in the computation of the metrics to avoid the edge effect (corner rounding). Three different line-widths, 30 nm, 50 nm, and 100 nm, are considered. The above simulation procedure is repeated for every possible combination of lithographic parameters.

The transfer function which describes the spatial distribution of exposure in the resist contributed by a beam is modeled based on the point spread function generated using a Monte Carlo simulation program SEEL[25] for the substrate system of 100 nm PMMA on Si and a beam energy of 50 keV. The point spread function is generated from a point source of 200,000 electrons. The point spread function includes the exposure profile due to the forward scattering and back scattering of electrons as in Fig. 4.2.[26]

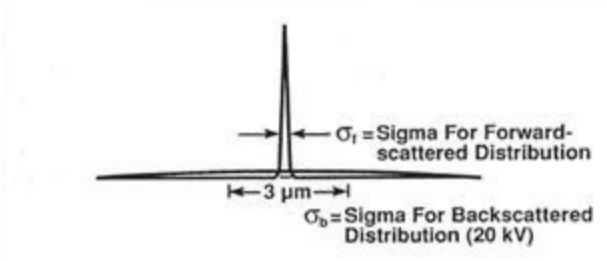

Figure 4.2: The electron scattering profile including the effect from the forward scattering and the back scattering of electrons.

From the point spread function, the total exposure and forward scattering range (the standard deviation of Gaussian) are extracted in each resist layer by curve fitting in the MATLAB. In Fig. 4.3, the plot in solid line indicates the exposure distribution from SEEL sampled from the beam incidence to a radius of 15 nm to include most of the forward and backs scattering effects. The plot in dashed line indicates the point spread function reconstructed from the MATLAB. To determine the amplitude of the point spread function, only data points that are separated from the beam incidence by several nm are considered, since the forward scattering is a dominant factor for determining the amplitude as shown in Fig. 4.2. Most of the exposure profile from the electron back scattering effect is lost in this study. Some of the previous

studies include the electron back scattering effect in the point spread function by summing two Gaussian functions.[27–30]

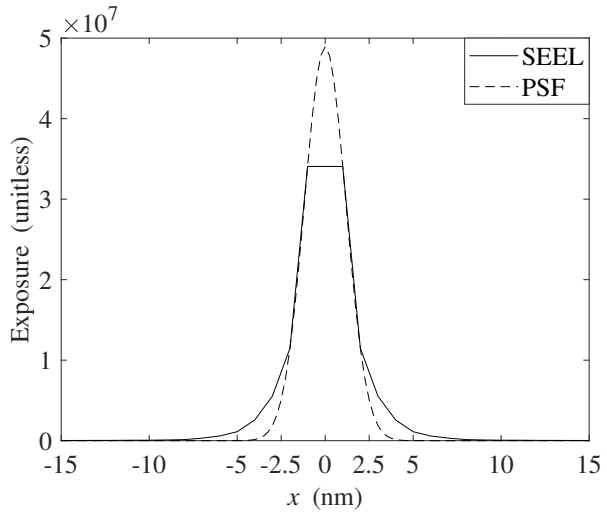

Figure 4.3: The standard deviation of Gaussian of the point spread function is extracted from the SEEL data using the MATLAB's curve fitting tool.

The ratios of the total energy and forward scattering range among the five resist layers form the basis of the transfer function as in Table 4.1. Then, the blurring factor for the middle layer is varied in the simulation (i.e., the blurring factors for the other layers are accordingly determined). The amplitude of the point spread function of a different layer is derived from the total energy conservation law as in Eq. 4.1 using the ratio from the Table 4.1.

Layer (nm)	20	40	60	80	100
Total energy (%)	106.4	104.5	100.0	92.9	86.1
σ (%)	98.3	98.8	100.0	101.8	101.2

Table 4.1: The layer dependent percentage ratios of the total energy and Gaussian standard deviation, σ of the point spread function.

$$A_1 * \frac{1}{2\pi\sigma_1^2} \int_{-\infty}^{\infty} e^{-\frac{x^2+y^2}{2\sigma_1^2}} dxdy = A_2 * \frac{1}{2\pi\sigma_2^2} \int_{-\infty}^{\infty} e^{-\frac{x^2+y^2}{2\sigma_2^2}} dxdy \tag{4.1}$$

As the study does not have direct electron scattering information from the square aperture beam, the scattering profile is approximated using the point spread function. The transfer function defines a different size and shape of the beam by a convolution of the point spread function with the aperture. Each of the simulation points of the aperture consists as a point source that forms a transfer function. According to the beam divergence, the spot size of the point spread function reduces as the distance from the resist increases when the beam energy is held constant. So, the study models the transfer function for smaller spot sizes from a point spread function with a smaller Gaussian standard deviation, σ. Then, the transfer function is obtained by convolving the point spread function with the corresponding aperture size. Table 4.2 lists the blurring factors used for the point spread function to generate the transfer function with different spot sizes.

B (nm)	σ (nm)			
2.5	0.25	0.5	0.75	1
5	0.5	1	1.5	2
10	1	2	3	4
20	2	4	6	8

Table 4.2: The blurring factors of the point spread function used for the transfer function for different spot sizes of beams.

The pattern location of the correction shot is controlled in respect to the *overlap coordinates* which is at the corner of the regular beams exposed area as in Fig. 4.4. The amount of overlap is measured in nm which is the base length of the square area formed from overlap. The overlap is 0 nm when the correction shot and the corner of the regular beam's exposed area touches as in Fig. 4.4(a). Positive overlap forms when the correction shot overlaps with the mentioned scalar amount. Negative overlap forms when the correction shot does not actually overlap. However, a negative amount of overlap measures the amount of the base distance of the square area between the corners of the correction shot and the regular beam's exposed area. The example overlap of 1 nm and -1 nm is in Fig. 4.4(b) and Fig. 4.4(c), respectively.

The simulated development time for the feature is chosen to profile a consistent line width for all the resist layers for the corner correction. The following figures Figs. 4.5(a-c) show the three dimensional feature development for different development times of 39s, 48s, and 60s where the longer development time duration results in a longer feature width at the bottom layer. The dimension of the simulated feature in Fig. 4.5 is chosen to reduce the memory usage for plotting in MATLAB. This is because corner rounding does not depend on the size of the line feature but the size of the beam patterned. The plotted feature is 60 nm length by 40 nm width where the beams are patterned without overlap when the size of the beam is B = 10 nm. The time evolution of the development shows that the shorter width development at the deeper layers would produce uneven correction at the deeper layers even when the shallower layer's correction is satisfactory. The correction shot result using a size of B_c = 2.5 nm square beam is presented in Figs. 4.5(d-f). The correction result from 39s of Fig. 4.5(d) indicates that the developing time is not enough for the correction shot to reach the deeper half of the features. Even when the correction shot reaches to the bottom layer, the correction for the feature developed shorter width at the deeper layers could be problematic because of having a dislocated ideal boundary from the shallower layer's ideal boundary. This result in the correction shot forming an island at the deeper layers as in Fig. 4.5(e). With a sufficient development time of 60s, the correction shot can develop into a larger size and fits well to the ideal boundary at the bottom layer so the corrected feature edge becomes smooth along the feature edges as in Fig. 4.5(f). Thus, the feature needs to be developed for 60 seconds of duration for the study.

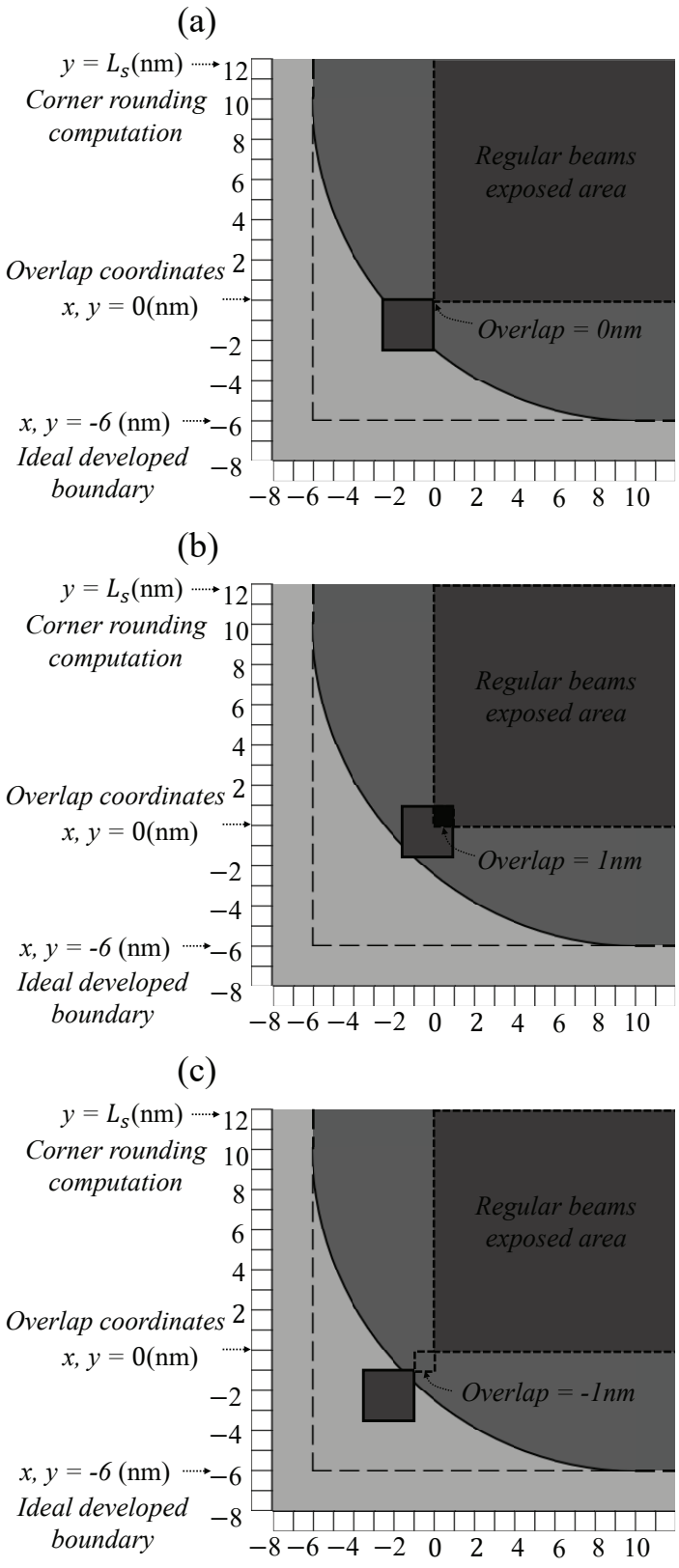

Figure 4.4: In the simulation, the amount of overlaps between the correction shot and the regular beams exposed area is evaluated in terms of the overlap coordinates. (a) Overlap = 0 nm, (b) overlap = 1 nm, and (c) overlap = -1 nm.

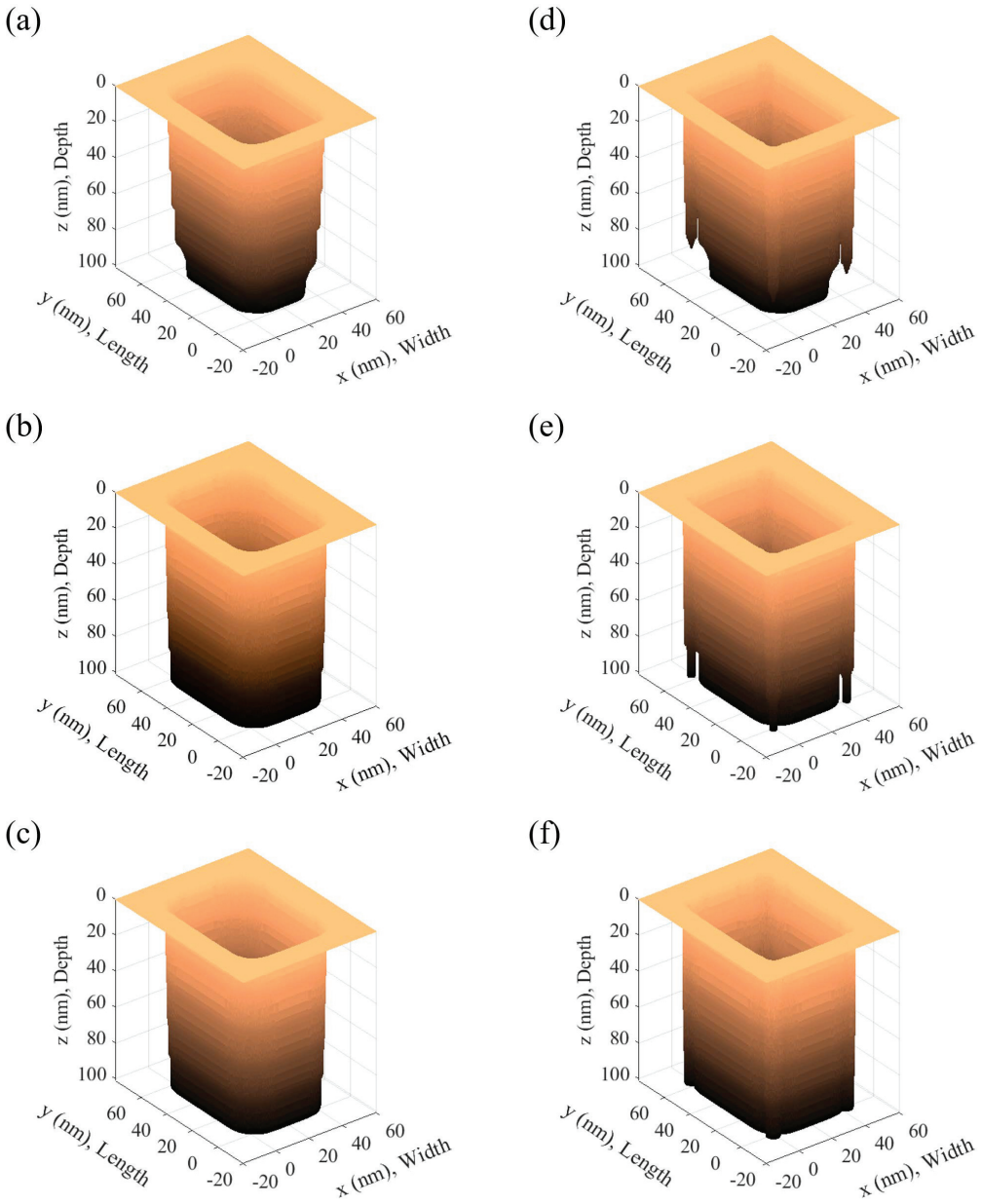

Figure 4.5: The time evolution of correction results using B_c = 2.5 nm sized square correction shot where the feature is written by a regular shot of B = 10 nm sized square shot. The three dimensional plot of the developed feature before the correction is presented in (a) 39s, (b) 48s, (c) 60s and after the correction is presented in (d) 39s, (e) 48s, and (f) 60s.

Chapter 5

Results and Discussion

The simulation results for the system with no faulty beam are presented first, followed by the results for a faulty system. All of the quality metrics are evaluated at the bottom layer of resist, to ensure that the feature is fully developed. Note that the metrics would show the similar tendencies at other layers.

5.1 Exposure Contrast

The exposure contrast is analyzed as a function of the exposing interval and blurring factor. The results for three line-widths are provided in Table 5.1 and Fig. 5.1. The exposure contrast is larger for a larger exposing interval. A smaller exposing interval results in a larger overlap between the (directly exposed) regions of adjacent points (refer to Fig. 2.1). A larger overlap allows for a more gradual exposure variation over the boundary of a feature due to a higher level of smoothing. Note that such smoothing does not occur when $I_e = B$, i.e., no overlap. The exposure contrast is smaller for a larger blurring factor (σ). The transfer function with a larger blurring factor decreases slower from its maximum, leading to a smaller change of exposure over the feature boundary. The line-width does not affect the exposure contrast. The exposure distribution over the feature boundary is not dependent on the feature size as long as the beam size, B, is smaller than the feature size.

I_e (nm)	σ (nm)			
	1	2	3	4
1	0.10	0.087	0.081	0.078
2	0.14	0.10	0.091	0.085
5	0.30	0.16	0.12	0.10
10	0.50	0.28	0.19	0.15

(a)

I_e (nm)	σ (nm)			
	1	2	3	4
1	0.087	0.074	0.069	0.066
2	0.12	0.09	0.079	0.073
5	0.27	0.15	0.11	0.095
10	0.49	0.27	0.18	0.14

(b)

I_e (nm)	σ (nm)			
	1	2	3	4
1	0.078	0.066	0.062	0.059
2	0.11	0.082	0.071	0.066
5	0.26	0.14	0.10	0.088
10	0.49	0.27	0.18	0.14

(c)

Table 5.1: The exposure contrast for the line-width (W) of (a) 30 nm, (b) 50 nm, and (c) 100 nm: the exposure contrast is normalized to the average exposure within the line.

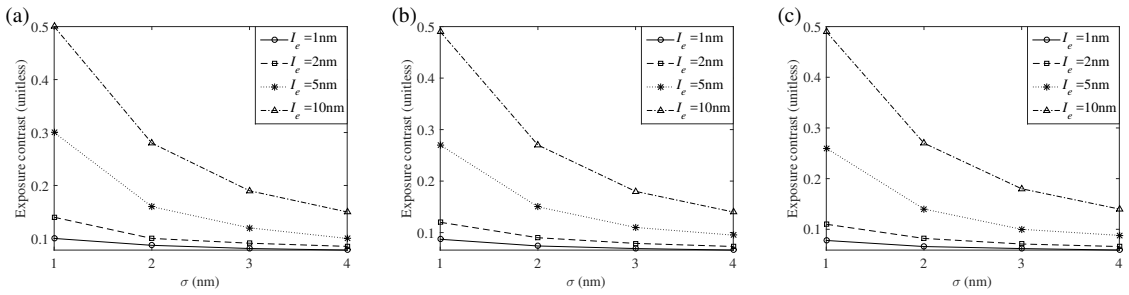

Figure 5.1: The exposure contrast for the line-width (W) of (a) 30 nm, (b) 50 nm, and (c) 100 nm: the exposure contrast is normalized to the average exposure within the line.

5.2 Exposure Variation

The spatial variation of the exposure within the feature is provided in Table 5.2 and Fig. 5.2. The exposure variation is smaller for a larger exposing interval (when $I_e \leq B$). When the exposing interval is smaller, the exposure drops gradually from the maximum level of the flat (plateau) region over a longer distance to a lower level, compared to the case of a larger exposing interval as can be seen in Fig. 5.3. This makes the exposure variation larger. The exposure variation decreases as the blurring factor increases when the exposing interval is relatively smaller. When the exposing interval is smaller, the flat region is narrower and the exposure difference between the flat region and feature boundary is larger. As the blurring factor increases, the exposure distribution tends to spread, making the exposure difference and therefore the exposure variation smaller. However, when the exposing interval is larger, the exposure-spreading effect due to the increased blurring factor diminishes. On the other hand, the exposure fluctuation (see Fig. 3.1) increases with the blurring factor, which eventually makes the exposure variation increase as seen in the case of $I_e = B$.

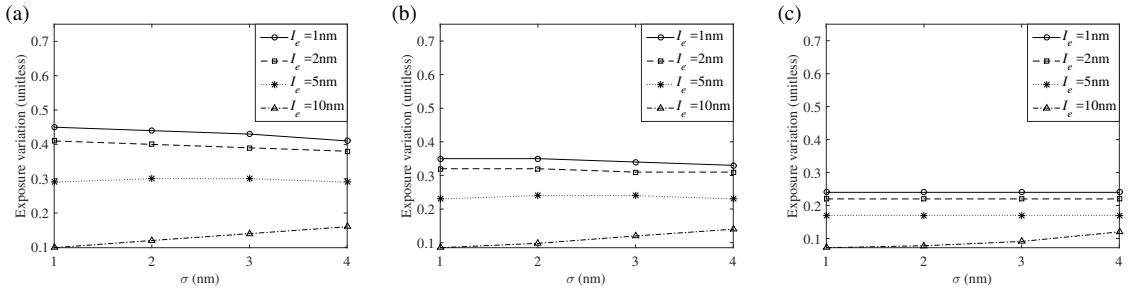

Figure 5.2: The exposure variation for the line-width (W) of (a) 30 nm, (b) 50 nm, and (c) 100 nm: the exposure variation is normalized to the average exposure within the line.

I_e (nm)	σ (nm)			
	1	2	3	4
1	0.45	0.44	0.43	0.41
2	0.41	0.40	0.39	0.38
5	0.29	0.30	0.30	0.29
10	0.099	0.12	0.14	0.16

(a)

I_e (nm)	σ (nm)			
	1	2	3	4
1	0.35	0.35	0.34	0.33
2	0.32	0.32	0.31	0.31
5	0.23	0.24	0.24	0.23
10	0.085	0.098	0.12	0.14

(b)

I_e (nm)	σ (nm)			
	1	2	3	4
1	0.24	0.24	0.24	0.24
2	0.22	0.22	0.22	0.22
5	0.17	0.17	0.17	0.17
10	0.072	0.078	0.091	0.12

(c)

Table 5.2: The exposure variation for the line-width (W) of (a) 30 nm, (b) 50 nm, and (c) 100 nm: the exposure variation is normalized to the average exposure within the line.

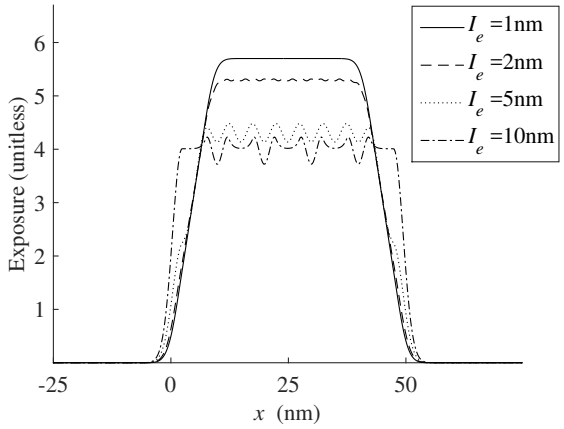

Figure 5.3: The exposure distribution along the width dimension at the middle layer of resist when W = 50 nm and σ = 2 nm.

The exposure variation is smaller for a larger feature (line-width). The relative size of the flat region (compared to the feature size) is larger and the effect of the exposure drop in the boundary region becomes relatively less as the feature size increases. This leads to a smaller exposure variation, and the relative exposure fluctuation (compared to the average exposure level) becomes smaller for a larger feature.

If I_e is increased beyond B, the exposure fluctuation becomes dominant, compared to the exposure drop in the boundary region. The exposure fluctuation increases as the exposing interval increases while $I_e > B$. Therefore, the exposure variation would increase with I_e (unless $I_e \gg B$).

5.3 Total Dose

The total dose required to achieve the target line-width at the bottom layer is examined for three line-widths and the results are provided in Table 5.3 and Fig. 5.4. Except for the line-width of 30 nm, the total dose increases as the exposing interval decreases or the blurring factor decreases in the case of I_e = 1 nm. A smaller exposing interval, or a smaller blurring factor with a small exposing interval, results in a narrower flat region in the exposure distribution and a larger exposure difference between the flat and boundary regions. With such an exposure distribution, the resist needs to be developed faster vertically in the flat region to reach the target boundary at the bottom layer through the lateral development. A relatively longer time is spent in the lateral development than in the vertical development due to the less-balanced spatial distribution of exposure. In such a case, the dose is less effectively used for the resist development and, therefore, a higher total dose is required.

I_e (nm)	σ (nm)			
	1	2	3	4
1	1.09	1.06	1.04	1.03
2	1.02	1.04	1.04	1.04
5	1.00	1.00	1.04	1.08
10	1.07	1.08	1.09	1.09

(a)

I_e (nm)	σ (nm)			
	1	2	3	4
1	1.20	1.17	1.14	1.13
2	1.09	1.12	1.12	1.11
5	1.01	1.01	1.05	1.09
10	1.00	1.01	1.03	1.02

(b)

I_e (nm)	σ (nm)			
	1	2	3	4
1	1.33	1.30	1.27	1.25
2	1.20	1.23	1.22	1.22
5	1.07	1.07	1.11	1.16
10	1.00	1.01	1.03	1.02

(c)

Table 5.3: The total dose for the line-width (W) of (a) 30 nm, (b) 50 nm, and (c) 100 nm: the total dose is normalized to the lowest total dose required.

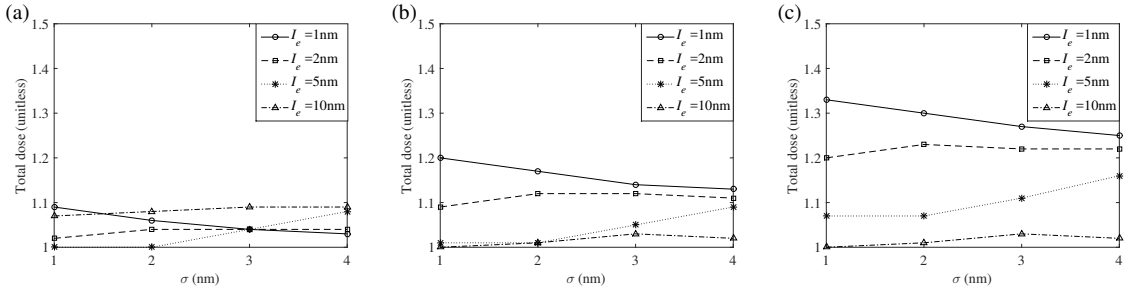

Figure 5.4: The total dose for the line-width (W) of (a) 30 nm, (b) 50 nm, and (c) 100 nm: the total dose is normalized to the lowest total dose required.

However, when the feature size is smaller, the aspect ratio, i.e., the ratio of resist thickness to feature size, is larger and less lateral development is needed. Hence, a less-balanced spatial distribution of exposure, where the exposure is higher at the center of a feature and decreases toward the feature boundary, does not lead to a lower efficiency in the resist development. This

explains why the total dose does not increase with the exposing interval when the line-width is 30 nm.

5.4 Dose Latitude

The dose latitude is provided for three line-widths in Table 5.4 and Fig. 5.5. When the average exposure levels in the flat and boundary regions are the same or similar between two cases, the dose latitude is larger in the cases where the exposure contrast is larger. This explains the observation that the dose latitude is larger for a smaller blurring factor with the exposing interval fixed. Another factor affecting the dose latitude is the exposure difference between the flat and boundary regions (see Fig. 5.3). When the exposure difference is larger, the edge location is affected less by the exposure distribution in the boundary region. Therefore, as the dose changes, the edge location moves less, i.e., a larger dose latitude. When the exposing interval increases, the exposure contrast increases, but the exposure difference decreases. The reason why the dose latitude is smaller for a larger exposing interval is that the effect of the exposure difference is larger than that of the exposure contrast.

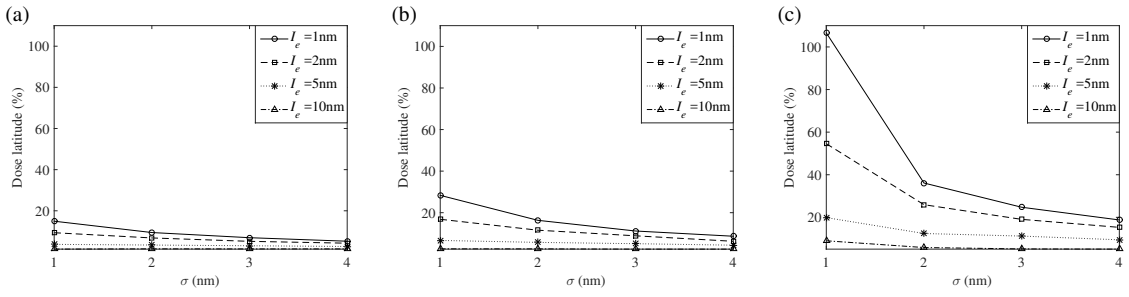

Figure 5.5: The percent dose latitude (%) for the line-width (W) of (a) 30 nm, (b) 50 nm, and (c) 100 nm: the dose latitude is computed relative to the dose required to achieve the target line-width.

I_e (nm)	σ (nm)			
	1	2	3	4
1	14.94	9.43	6.92	5.21
2	9.34	6.80	5.15	4.25
5	3.68	3.35	3.00	2.65
10	1.36	1.50	1.46	1.47

(a)

I_e (nm)	σ (nm)			
	1	2	3	4
1	28.34	16.32	11.18	8.67
2	16.83	11.57	8.87	6.23
5	6.65	5.71	5.08	4.36
10	2.60	2.59	2.46	2.46

(b)

I_e (nm)	σ (nm)			
	1	2	3	4
1	106.58	36.11	24.74	18.77
2	54.57	25.93	19.05	15.29
5	19.87	12.41	11.20	9.45
10	8.99	5.82	5.17	5.07

(c)

Table 5.4: The percent dose latitude (%) for the line-width (W) of (a) 30 nm, (b) 50 nm, and (c) 100 nm: the dose latitude is computed relative to the dose required to achieve the target line-width.

5.5 LER and Maximum Indent

The LER and maximum indent measured along the length dimension for the line-width of 50 nm are provided in Table 5.5 and Fig. 5.6. A typical source of LER is the stochastic fluctuation of exposure. However, as pointed out earlier, the LER and maximum indent in Fig. 5.6 are due to the periodic variation of deterministic exposure. Such variation can be substantial depending on the shape of transfer function and exposing interval. It is seen that the LER and maximum indent are small, but not negligible. They decrease as the exposing interval decreases since the exposure distribution tends to be smoothed out. The largest LER and maximum indent are obtained when both exposing interval and blurring factor are largest. This is because the exposure fluctuation is maximized in that case.

I_e (nm)	σ (nm)			
	1	2	3	4
1	0	0	0	0
2	0.039	0.020	0.0095	0
5	0.11	0.18	0.17	0.028
10	0.35	0.34	0.43	0.62

(a)

I_e (nm)	σ (nm)			
	1	2	3	4
1	0	0	0	0
2	0.053	0.029	0.021	0
5	0.25	0.29	0.29	0.057
10	0.94	0.72	0.96	1.14

(b)

Table 5.5: (a) LER and (b) maximum indent in nm for the line-width (W) of 50 nm.

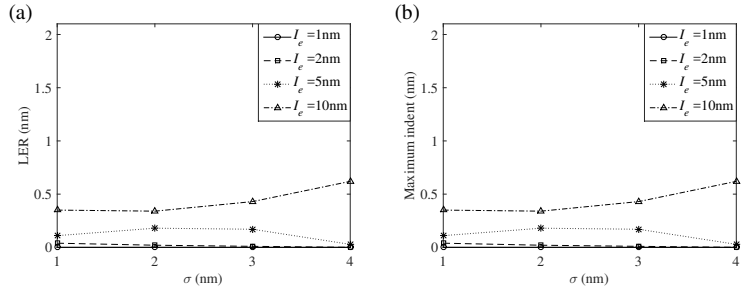

Figure 5.6: (a) LER and (b) maximum indent in nm for the line-width (W) of 50 nm.

5.6 Corner Rounding

The corner rounding results of a single line of a feature exposed by a uniform dose of B = 10 nm square regular shot at an exposing interval of $I_e = B$ = 10 nm is in Table 5.6, Fig. 5.7, and Fig. 5.8. For the transfer function with a blurring factor from 1 nm to 4 nm, the area of the corner rounding increases as the blurring factor increases as in Table 5.6 and Fig. 5.7. The corner rounding enlarges as the depth increases because the feature width decreases compared to the width development at the shallower depth. Fig. 5.8 shows the corner rounding at the middle layer for a blurring factor from 1 nm to 4 nm. The corner rounding becomes larger as the σ enlarges due to the shape of the transfer function which has a larger area of non-ideal distribution as the σ increases. The rounded corner development is due to the exposure shape at

the corner of the feature that decreases radially from the peak exposure region from the center of the beam. The sub-figures (a-d) of Figs. 6.16, 6.17, 6.19, and 6.21 shows the rate distribution at the corner of the feature and the corner rounding at the top, middle, and bottom layer for the transfer function with a blurring factor (σ) from 1 nm to 4nm.

Corner rounding (nm)	σ (nm)			
	1	2	3	4
Top layer (16 nm)	1.48	5.66	11.73	20.24
Middle layer (52 nm)	1.48	5.71	12.40	21.16
Bottom layer (100 nm)	1.47	5.70	12.30	21.34
Total	4.42	17.07	36.43	62.74

Table 5.6: The corner rounding (nm^2) for the spot size, B = I_e = 10 nm.

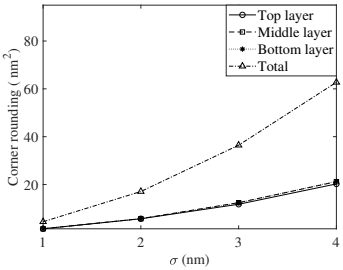

Figure 5.7: The corner rounding (nm^2) for the spot size, B = 10 nm for the line-width (W) of 50 nm.

The corner rounding of the *exposing intervals* that are less than the beam size is not analyzed in this study and is saved for future corner correction work. The corner development result of the case of $I_e = B$ is chosen as a reference for the correction because it produces the smallest corner rounding result among the rest of the writing strategies in this study. This is because in the case of $I_e < B$, the exposure contrast at the corner is minimized when the *exposing interval* decreases. The resulting exposure rounding is significant in that the exposure contrast from the writing strategy dominates the outcome more than the shape of the transfer function, so the corner rounding is much larger than the case of $I_e = B$.

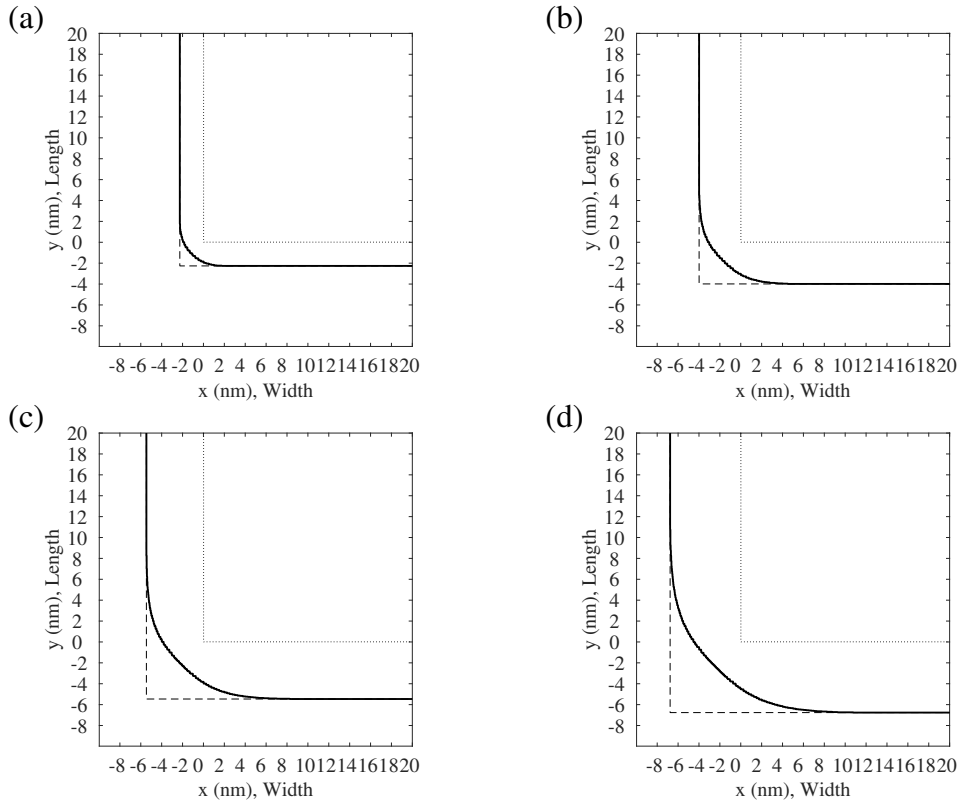

Figure 5.8: The development contour at the middle layer of the corner of the feature where the feature is exposed by a regular shot at an interval of $I_e = B$ = 10 nm is shown: (a) σ = 1 nm, (b) 2 nm, (c) 3 nm, and (d) 4 nm. The beam exposed boundary (dotted), ideal developed boundary (dashed), and the actual developed boundary (solid) is indicated.

Chapter 6

Solution

6.1 Effect of Overlap Beam Patterning

Pattern delineation in the vicinity of the corner of the feature typically requires increasing the level of exposure by overlapping shots near the corner so that it would develop closer to the ideal feature corner. However the directivity of a shot depends more on the size of the correction shot than the amount of overlap. The size of the shot determines the consistency of the correction at the feature corner over the deeper layers. An overlap aids development along the boundary of the rounded corner which is in a 90° opposite direction of a directive development as in Fig. 6.1. The shape and size of the transfer function impacts a directive correction over the depth of the feature. In the next section, the size of the correction shot is determined so that the shot can bring the maximum directivity.

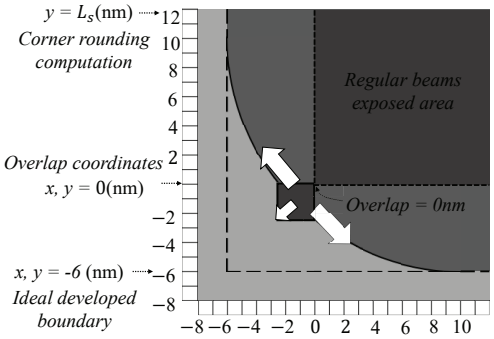

Figure 6.1: In this illustration, a single shot is patterned with an overlap exposure. An overlap would aid development in a 90° opposite direction toward the corner of the ideal feature boundary.

6.2 Effect of a Beam Size on Directive Correction at Varying Depth

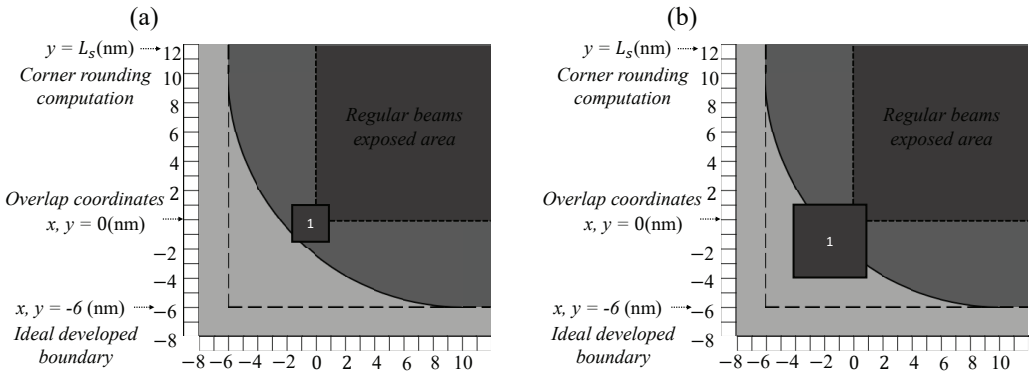

Figure 6.2: In this illustration, a single correction shot is applied at the corner of the feature where the size is (a) B_c = 2.5 nm square and (b) B_c = 5 nm square. Both shots are overlapped with a 1 nm x 1 nm square area to the regular beam exposed area of the feature.

A larger size correction shot is capable of transferring a more directive shape than a smaller size shot when it is overlapped the same amount at the corner of the regular beam exposed area as in Fig. 6.2. The larger shot corrects more area and corrects closer to the ideal corner at the shallower layers than the smaller shot as in Fig. 6.3. However, overlapped exposure increases development along the already developed edges which is in the direction of anti-diagonal of the ideal feature corner. An anti-diagonal direction of development would eventually overdevelop outside of the ideal feature boundary over the shallower layers before the corner of the deeper layers are corrected. To avoid overdeveloped correction shape at the shallower layers, the larger correction shot requires a lower level of dose usage as the size of the correction shot increases. The correction shot using a low dose would not develop or transfer partially of its intend size over the deeper layers which subsequently makes unable to transfer the shot closer to the feature corner. Also, the directivity gets worse as the correction shot broadens.

The following Fig. 6.3 compares the correction results of a 2.5 nm size square correction shot and a 5 nm size square correction shot on a feature written by a 10 nm square shot in a sharpness of Gaussian σ of 4nm. Both correction shots are overlapped with an identical amount of 1 nm square area with the regular beam exposed area. Both correction shots used the highest amount of dose so that each would produce the best area reduction at the top layer

without resulting any over development at the top layer. The dose level used for the 2.5 nm square shot is a normalized dose of 1.3 as compared to the 10 nm square shot. The 5 nm square correction shot used a normalized dose of 0.4 to produce a similar smooth correction at the side of the feature on the top layer. The development results from Fig. 6.3 show that the larger correction shot is more directive at the shallower layers and dose usage is efficient. However, the development results at the deeper layers inevitably suffer both toward the ideal corner and a little along the side of the feature from using a low level of dose.

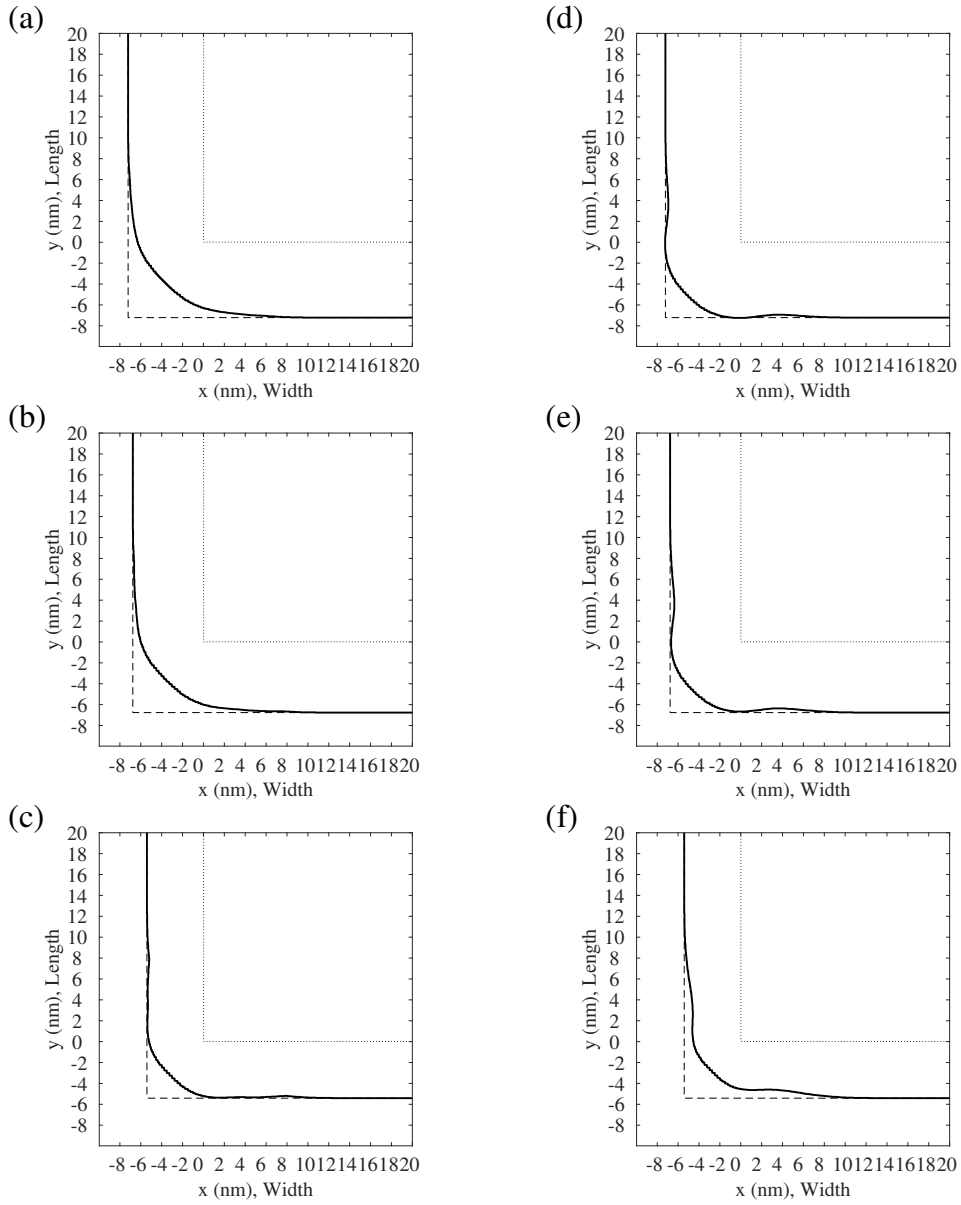

Figure 6.3: A single shot correction results using a 2.5 nm square shot in (a), (b), and (c) and a 5nm square shot in (d), (e), and (f) when the both shots are overlapped with a 1 nm x 1 nm square area with the regular beam exposed area. $B = I_e$ = 10 nm and σ = 4 nm.

In order to improve the correction at the deeper layers, it is necessary to use a higher dose when a larger size of correction shot is used. If multiple beams are used to improve the feature corner, a larger sized correction shot's directiveness suffers at the deeper layers. Using a low level of dose to avoid overdevelopment at the side of the feature over the shallower layers, the larger sized correction shot produces less directive development at the corner. Fig. 6.4 illustrates an additional second shot given to the single shot correction result in respect to the development at the bottom layer. In the figure, both shots are overlapped -2 nm from

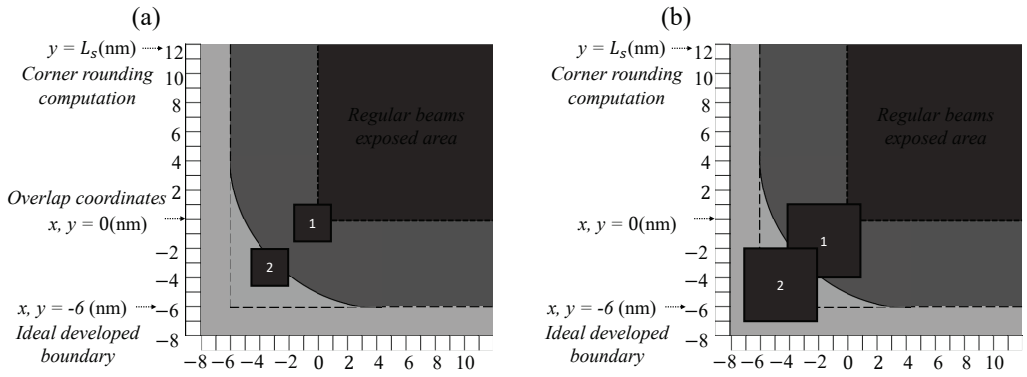

Figure 6.4: In this illustration, two correction shots are applied at the corner of the feature where the size is (a) B_c = 2.5 nm square and (b) B_c = 5 nm square. The second shots are overlapped with a -2 nm x -2 nm square area to the regular beam exposed area of the feature.

the regular beam exposed area. Every additional shot has to use much lower dose than the previous patterned shot to avoid any over development at the side of the feature. This is because the remaining corner rounding area becomes much smaller especially at the shallower layers after the previous shot is patterned. Consequently, a lower dose would reduce transferring the additional shot's correction effect at the deeper layers.

In Fig. 6.5, the correction results due to two shots are shown where one more shot of a same size is added to the single shot correction result of the above Fig. 6.3. Both second shots use a normalized dose of 0.2. As a result, the 2.5 nm square shots correction has the corner directivity improvement over the entire depth as in Fig. 6.5 (a-c) and is corrected best at the bottom layer. The same amount of dose is high enough for the 5 nm square shot correction that the feature over develops at the side of the feature to the middle layer as in Fig. 6.5 (d-e). However, the dose level is not high enough to improve the corner at the bottom layer from the single shot's correction result. The bottom layer's correction result after the second shot exposure is as shown in Fig. 6.5(c). So in order not to exceed development outside of the ideal boundary, the larger correction shot needs to use a much lower dose level than the normalized dose of 0.2 for the second shot. Then, the larger shot's correction at the deeper layers would be worse than the result using the dose level of 0.2. Thus, using a larger correction shot has a limitation on improving directive corner correction. Therefore, a smaller shot of 2.5 nm square beam is implemented for a directive correction in this study.

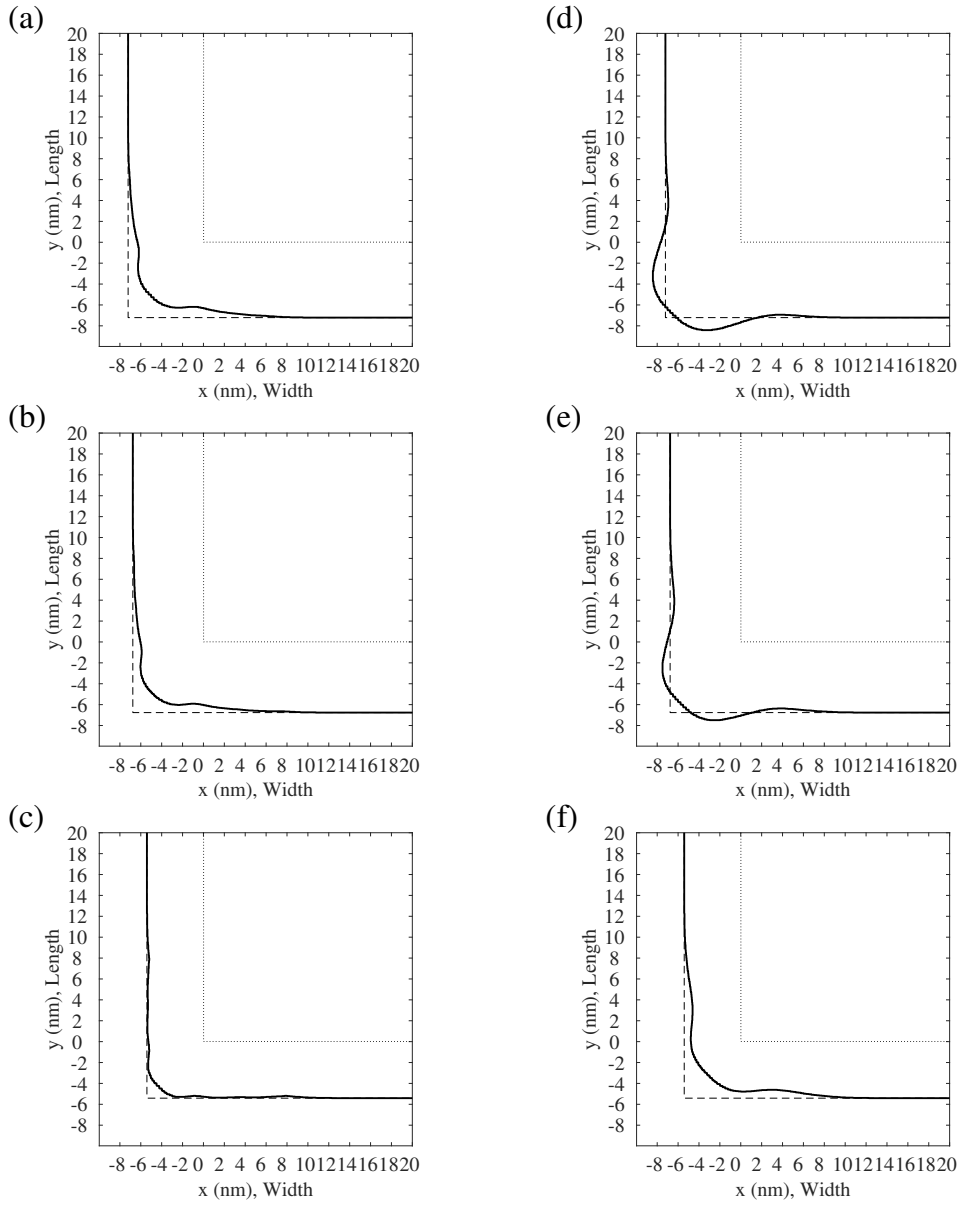

Figure 6.5: Two shots correction results using a B_c = 2.5 nm square shots in (a), (b), and (c) and a B_c = 5 nm square shot in (d), (e), and (f) when the second shot is overlapped of -2 nm x -2 nm square area with the regular beam exposed area. $B = I_e$ = 10 nm and σ = 4 nm.

6.3 Proposed Correction Strategy

This study corrects the rounded corner of the feature by serially patterning a shot that is $\frac{1}{4}$ of the regular shot from outside of the beam exposed area toward the ideal corner of the feature. The method could also correct a feature whose width develops shorter than expected as the depth of the feature increases. This is realized by controlling the depth of the correction shot to be patterned by giving an adequate level of dose. The corner directivity at different

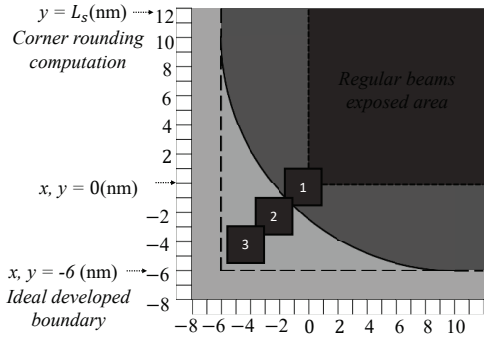

Figure 6.6: In this illustration, three correction shots are serially patterned from outside of the corner of the regular beam exposed area toward the ideal corner of the feature. The correction shot used is a B_c = 2.5 nm square beam and the regular shot used for the feature is B = 10 nm square beam. $B = I_e$ = 10 nm.

depths is achieved by decreasing the level of dose of each shot that is away from the center of the feature. This way the patterned shots by target depth could occupy the required area of corner correction. As in Fig. 6.6, the top layer requires all shots of 1, 2, and 3 to be developed, the middle layer requires shot 1 and 2, and the bottom layer requires shot 3 to be developed. Ultimately, the shot 1 targets all the layers, the shot 2 targets top to middle layers, and the shot 3 targets only top layers.

The amount of overlap between each of the shots and the regular beam exposure area needs to be determined when the correction aims to smooth the edge of the feature while minimizing any undeveloped area. The efficiency of the correction shot depends on shot 1 which is the innermost located shot among the correction shots patterned. Shot 1's role is to evenly shape the correction pattern smoothing the entire depth of the feature. The correction of shot 1 is explained in detail in the next section.

6.4 Amount of Overlap and the Corresponding Developmental Trade-off Characteristic

This section explains how the amount of overlap determines the corner directiveness. A small spot sized beam has the ability to confine the energy deposition due to the size of the beam. The correction may leave out some of the corner areas that needs to be corrected. Thus, an adequate amount of overlap needs to be chosen to reduce a lack of development near the corner after the correction.

The following Fig. 6.7 shows the rate distribution before and after a correction shot is patterned when the amount of overlap of the correction shot is -1 nm as from the Table 6.1 when σ = 4 nm. (a) shows the rate distribution at the middle layer of one corner of the feature before the correction. The green circle in (a) and (c) indicate the corner rounding region bounded by x = -2 nm to x = -6 nm and y = -2 nm to y = -6 nm matching the developed contour in (c). The developed edges in (c) is initiated from the round black dot of the peak value in (a) and laterally develop to the final developed edges in (c) toward the direction of the blue arrows which stops at the cross shaped black dots in (a).

Fig. 6.7 (b) shows the rate distribution at the middle layer of one corner of the feature after the correction shot is patterned in the green circle region of (a). As a result, the green circle region in (a) is replaced by a peaked mountain shaped energy. An additional development path is created indicated by a red arrow initiated from the peak point of the correction shot's energy. However, the exposure increases the energy deposition at the region of exposure but not at the outside of the correction shot's area. The resulting development in (d) shows that the side of the feature which was previously part of the corner rounding region is still not developed as indicated in the green circles. Although correction with decreased amount of overlap could pattern closely to the ideal corner, it could produce some correction shape defect. For a small spot sized beam, the focused energy transfer would result in a decrease of the correction directivity as the amount of overlap increases. The corner directivity reduction is indicated by the % area reduction in Table 6.1.

A larger amount of overlap maximizes development at the side of the feature and is capable of producing a smooth or consistent correction shape to the deeper layers at a cost of the directiveness of the correction. A larger overlap with the feature increases the correction shot's energy more than when it is overlapped closer to the ideal feature corner. Most of the correction region at the side of the feature at the deeper layers are above the development threshold. If the correction shot is overlapped less with the feature, then the composite energy of the correction shot is significantly lower which may be mostly below the development threshold, especially at the deeper layers.

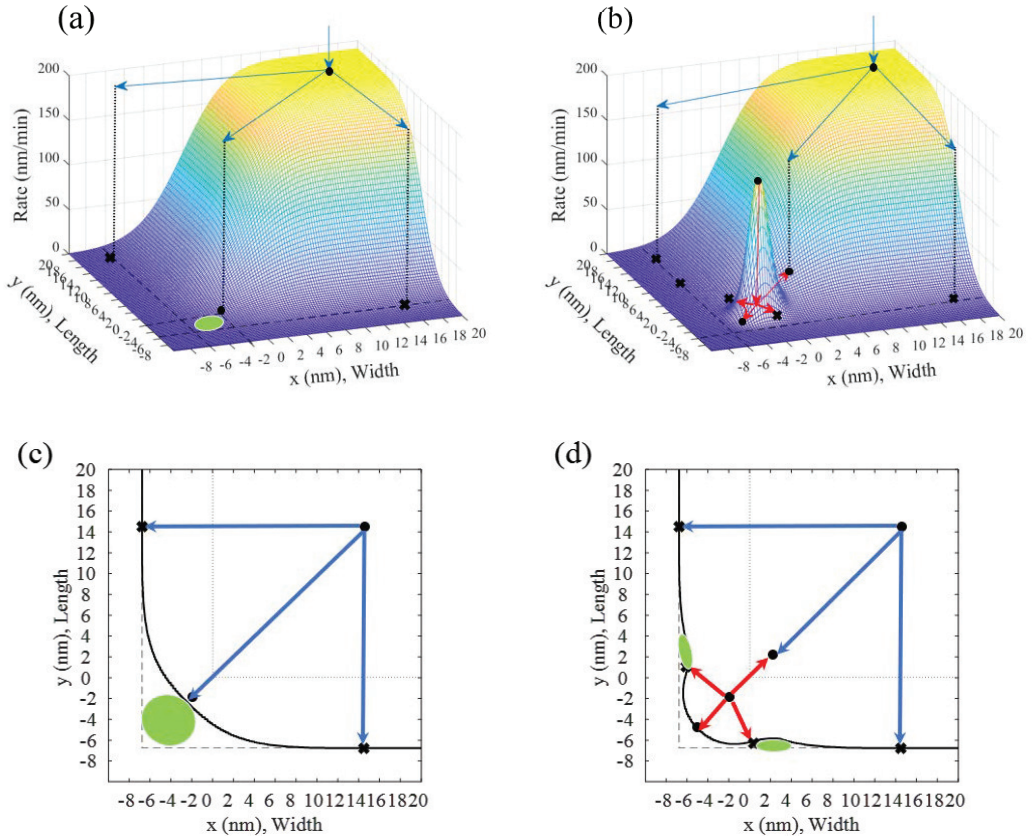

Figure 6.7: The rate distribution at the middle layer of one corner of the feature (a) before and (b) after the correction shot is overlapped of -1 nm to the feature corner. I_e = B = 10 nm, σ = 4 nm, and W = 50 nm. The corner rounding is indicated as in green circle in (c). After correction, the corner rounding region is not fully corrected in (d) due to the small spot size of the correction shot.

Overlap (nm)	Dose	Top		Middle		Bottom	
		% area reduced	Over developed area (nm^2)	% area reduced	Over developed area (nm^2)	% area reduced	Over developed area (nm^2)
-1	1.3	-52.25	0	-59.10	0	-68.49	0.70
0	1.3	-38.89	0	-48.29	0	-68.24	0
1	1.3	-29.32	0	-42.34	0	-71.90	0
2	1.3	-23.09	0	-39.88	0.45	-69.57	3.72

(a)

Table 6.1: The directivity and shape trade off for the correction shot are each indicated by the % area reduced and over developed area (nm^2), respectively. B = 2.5 nm, I_e = B = 10 nm, σ = 4 nm, and W = 50 nm.

The increasing development threshold when overlap is smaller is recognized by observing the level of the rate distribution of the correction shot along the corner development path. Figs.

6.9(a-c) each shows the overlap of 0 nm, 1 nm, and 2 nm when the correction shot's dose is given of 1.3 as in Table 6.1. Figs. 6.9(a-c) is sampled along the green line which is a diagonal line through the corner of the regular beam exposed area as in Figs. 6.9(d-f). In Fig. 6.9, The correction shot's peak level reduces from 2 nm to 0 nm. As the amount of overlap decreases, the deeper layers are exposed to a lower level of the peak rate so that the development from the correction shot would require less time to develop to the nearby pixels. So, the less the overlap, the area correction shot transferred to the deeper layers may decrease in size. This results in a poor development at the deeper layers either forming an island as in Fig. 6.8(b) or producing a defective correction shape as in Fig. 6.7(c).

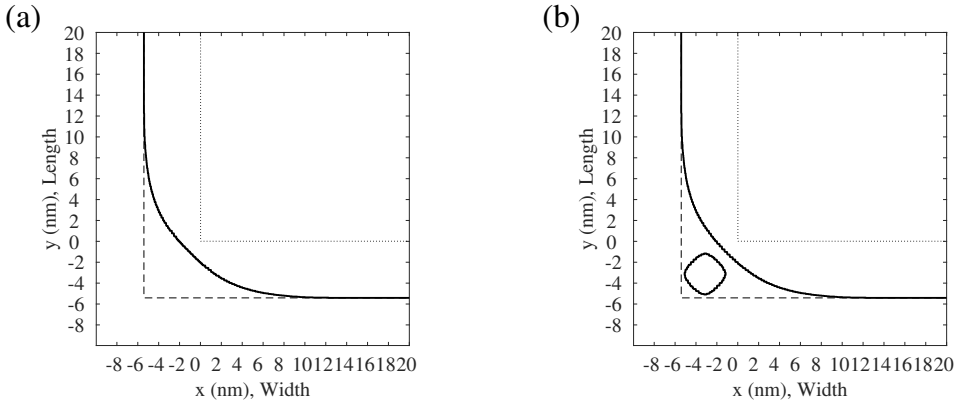

Figure 6.8: (a) The development result at the bottom layer before correction. (b) A single shot correction result using a B_c = 2.5 nm square shot when the the shot is overlapped with a -2 nm x -2 nm square area with the regular beam exposed area and the dose level used is 1.1. $B = I_e$ = 10 nm and σ = 4 nm.

As seen from the correction shape, the overlap of 2 nm would correct toward the ideal corner but, the amount is smallest among other amounts of overlap. The direcitivty arrows of blue and red arrow in Fig. 6.9(f) are spaced closer than the smaller overlaps in Figs. 6.9(d-e). Also, because the correction shape forms a shape that is not directive which forms a long stripe as indicated by the overdeveloped area of 3.72nm^2 at the bottom layer in Table .6.1, the overlap of 2 nm is identified an *overlap threshold* for the correction. Thus, it is eliminated for the correction choice. This turned out to be true for the entire simulated range of $I_e = B$ = 10 nm regular square beam's tf with σ = 1,2,3, and 4 nm.

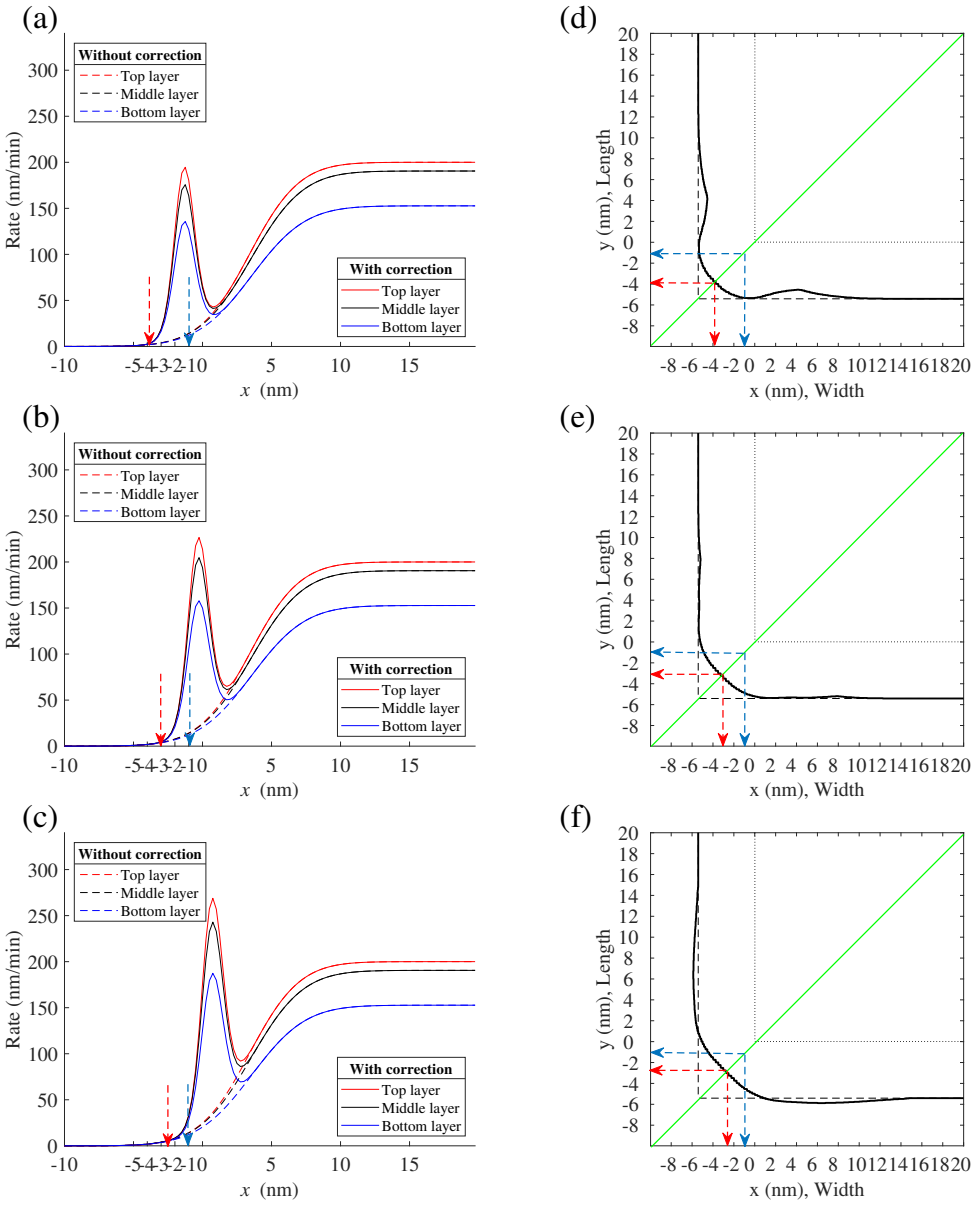

Figure 6.9: The rate distribution along the corner of the regular beam exposed area using a B_c = 2.5 nm square shot when overlapped with a (a) 0 nm x 0 nm square area, (b) 1 nm x 1 nm, and (c) 2 nm x 2 nm with the regular beam exposed area when the dose level is 1.3. Sub-figures (d), (e), and (f) is the correction result at the bottom of the layer of (a), (b), and (c), respectively. The rate distribution of (a), (b), and (c) is sampled along the green line in (d), (e), and (f). B = I_e = 10 nm and σ = 4 nm.

For the correction shots, shot 1 and 2 is to be overlapped that would fully develop the width of the feature at the corner just as the width development at the center of the feature. Shot 1 is chosen to overlap 1 nm which would produce a smooth feature edge and reduce the correction area as much as possible in respect to the bottom layer. The correction results of the top, middle, and bottom is in Figs. 6.10(d-f), where I_e = B = 10 nm and σ = 4 nm. Shot 1's dose level for

the three shot correction is in Table 6.2 where B_c = 2.5 nm and its tf's σ = 0.25, 0.5, 0.75, and 1 nm. In the Table, as the correction shot's sharpness decreases, the required dose level of the correction shot increases. This is because the broader the correction beams, the larger the areas can be affected. At a lower dose, most of the areas from the correction shot may not sufficiently develop at the deeper layers even when the shallower layers are fully developed. With the dose level in the Table 6.2, a consistent correction shape and size is transferred with directiveness even if the corrected corner edge may not be closest to the ideal corner of the feature. In the Table, although the % area reduction after the correction increases with depth the actual transferred shot size is consistent. In the Table, higher percentage of the area of the corner rounding is corrected. This is because, the correction shot is transferred relatively a consistent size over the entire depth but, the corner rounding area gets smaller at deeper depth due to shorter developed feature width.

Sigma (nm)	Overlap (nm)	Dose	Top		Middle		Bottom	
			% area reduced	Over developed area (nm)	% area reduced	Over developed area (nm)	% area reduced	Over developed area (nm)
0.25	1	0.13	-49.77	0	-56.01	0	-69.19	0
0.5	1	0.8	-29.85	0	-41.43	0	-69.30	0
0.75	1	1	-28.14	0	-40.40	0	-72.12	0
1	1	1.3	-29.32	0	-42.34	0	-71.90	0

Table 6.2: The correction choice of shot 1's amount of overlap, dose level, and the corresponding correction results at (a) top, (b) middle, and (c) bottom layers using a B_c = 2.5 nm square shot. $B = I_e$ = 10 nm and tf of the correction shot is of σ = 0.25, 0.5, 0.75, and 1 nm.

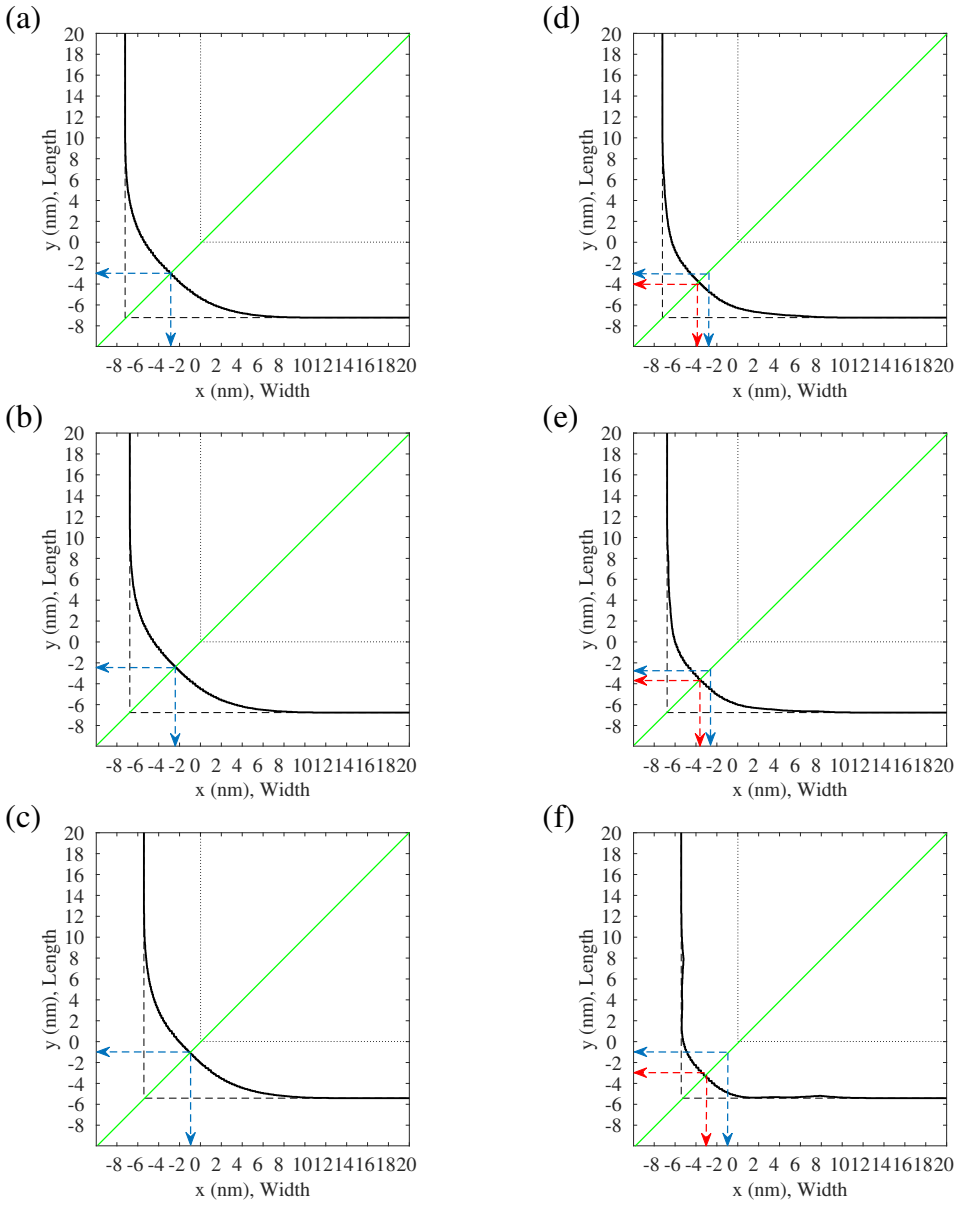

Figure 6.10: The development results before the correction at (a) top, (b) middle, and (c) bottom layer when σ = 4 nm. A single shot correction results after the correction at (d) top, (e) middle, and (f) bottom layer using a B_c = 2.5 nm square shot when overlapped with a 1 nm x 1 nm square area with the regular beam exposed area. $B = I_e$ = 10 nm and σ = 4 nm.

6.5 Correction Result after the Second Shot's Application

In the previous section, the amount of overlap of shot 1 is chosen so that it leaves some space for other shots to complete the correction. Shot 2's overlap and dose level is determined so that it maximizes development from the middle layer to the bottom layer. The amount of overlap is chosen to produce an anti-directive development that prioritizes improvement at the bottom layer's result of the shot 1's correction. An example choice of overlap amount for shot

2 when added to the previous section's example is shown in Fig. 6.11. The figure demonstrates the location of shot 2 with an overlap of -1 nm in (a-b), and -2 nm in (c-d) from the corner of the regular beam exposed area. The squares are 2.5 nm x 2.5 nm sized correction shot which each of the corner of each squares are spaced in 1 nm apart. The red shot in (a-d) represent the shot 1 with an overlap of 1 nm decided from the previous section. The green shot in (a-b) represents a candidate shot 2 with an overlap of -1 nm with the regular beam exposed area. The orange shot in (c-d) represents a candidate shot 2 with an overlap of -2 nm with the regular beam exposed area. The gray shots in (a-d) are beams that are not exposed but shown for illustrative purposes. The overlap amount refers to the amount between shot 2 and the regular corner shot of the feature, not between shot 1 and shot 2.

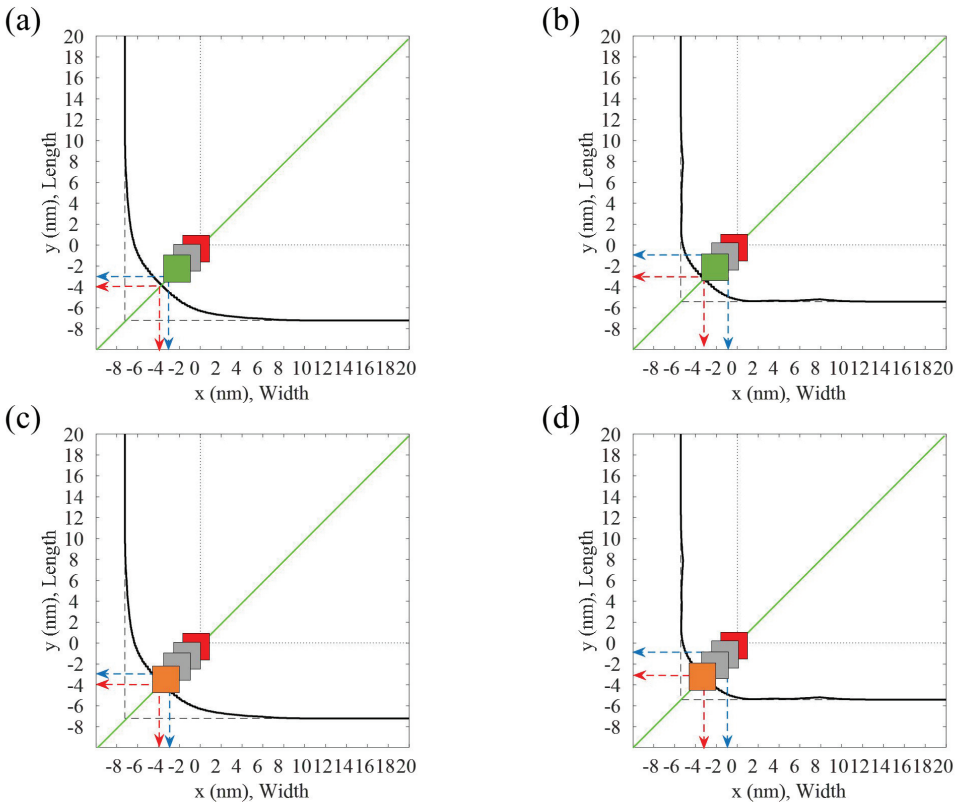

Figure 6.11: In this illustration, two correction shots are applied at the corner of the feature where the size is 2.5 nm x 2.5 nm square. The shot 1 is 1 nm x 1 nm overlapped (red square). The shot 2 candidates are overlapped with a -1 nm x -1 nm square area (green square) in (a) and (b) and -2 nm x -2 nm square area (orange square) in (c) and (d) to the regular beam exposed area of the feature.

The following Table 6.3 lists an overlap of 0 nm, -1 nm, -2 nm, and -3 nm with a possible dose combination. Overlap of 0 nm results in an overdevelopment because it is too close to shot 1 for the dose ranges in the tables. Therefore, it is eliminated. Same is applied to the dose levels for the overlap of -1 nm and -2 nm that results in an overdevelopment. A dose level higher than 0.2 is also discarded for the design choice. Then, the highest dose and overlap combination that results in best % area reduction is when the overlap is -2 nm with the dose level of 0.2. The results from an overlap of -3 nm with dose level of 0.2 and 0.3 have similar or better % area reduction result. However, the development shape leaves more undeveloped area at the side of the feature because it is closer to the ideal feature corner. The development at the side of the feature near the feature corner is maximized from increasing its exposure by overlapping the shot 2 more with the regular shot. For the 10 nm square beam with tf sharpness of σ = 1 nm, 2 nm, 3 nm, and 4 nm, the resulting choice of overlap amount of shot 2 and the regular beam exposed area is 0 nm, -1 nm, spaced -2 nm, and -2 nm, respectively as in Table 6.5. The resulting choice of overlap amount of shot 1 and shot 2 is 1.5 nm, 0.5 nm, spaced 0.5 nm, and 0.5 nm, respectively as in Table 6.4.

Overlap (nm)	Dose	Top		Middle		Bottom	
		% area reduced	Over developed area (nm^2)	% area reduced	Over developed area (nm^2)	% area reduced	Over developed area (nm^2)
0	0.1	-31.75	0	-46.37	0	-78.60	0.23
0	0.2	-33.88	0	-49.83	0	-82.18	0.99
0	0.3	-35.75	0	-53.43	0	-84.90	2.07

(a)

Overlap (nm)	Dose	Top		Middle		Bottom	
		% area reduced	Over developed area (nm^2)	% area reduced	Over developed area (nm^2)	% area reduced	Over developed area (nm^2)
-1	0.1	-36.87	0	-49.66	0	-78.78	0
-1	0.2	-41.48	0	-54.52	0	-84.33	0
-1	0.3	-44.63	0	-57.89	0	-88.56	0.028

(b)

Overlap (nm)	Dose	Top		Middle		Bottom	
		% area reduced	Over developed area (nm^2)	% area reduced	Over developed area (nm^2)	% area reduced	Over developed area (nm^2)
-2	0.1	-43.66	0	-54.47	0	-79.44	0
-2	0.2	-51.86	0	-62.91	0	-87.47	0
-2	0.3	-56.93	0	-68.42	0	-92.25	0.35

(c)

Overlap (nm)	Dose	Top		Middle		Bottom	
		% area reduced	Over developed area (nm^2)	% area reduced	Over developed area (nm^2)	% area reduced	Over developed area (nm^2)
-3	0.1	-43.19	0	-50.86	0	-74.36	0
-3	0.2	-57.49	0	-63.57	0	-78.32	0
-3	0.3	-65.91	0	-73.22	0	-84.79	0

(d)

Table 6.3: The correction result for the candidates of shot 2 with an amount of overlap of (a) 0 nm, (b) 1 nm, (c) 2 nm, (d) -3 nm square area with the regular beam exposed area at a dose level of 0.1, 0.2, and 0.3. The corresponding correction results at the top, middle, and bottom layers are presented. B = I_e = 10 nm and tf of the correction shot is σ = 4 nm.

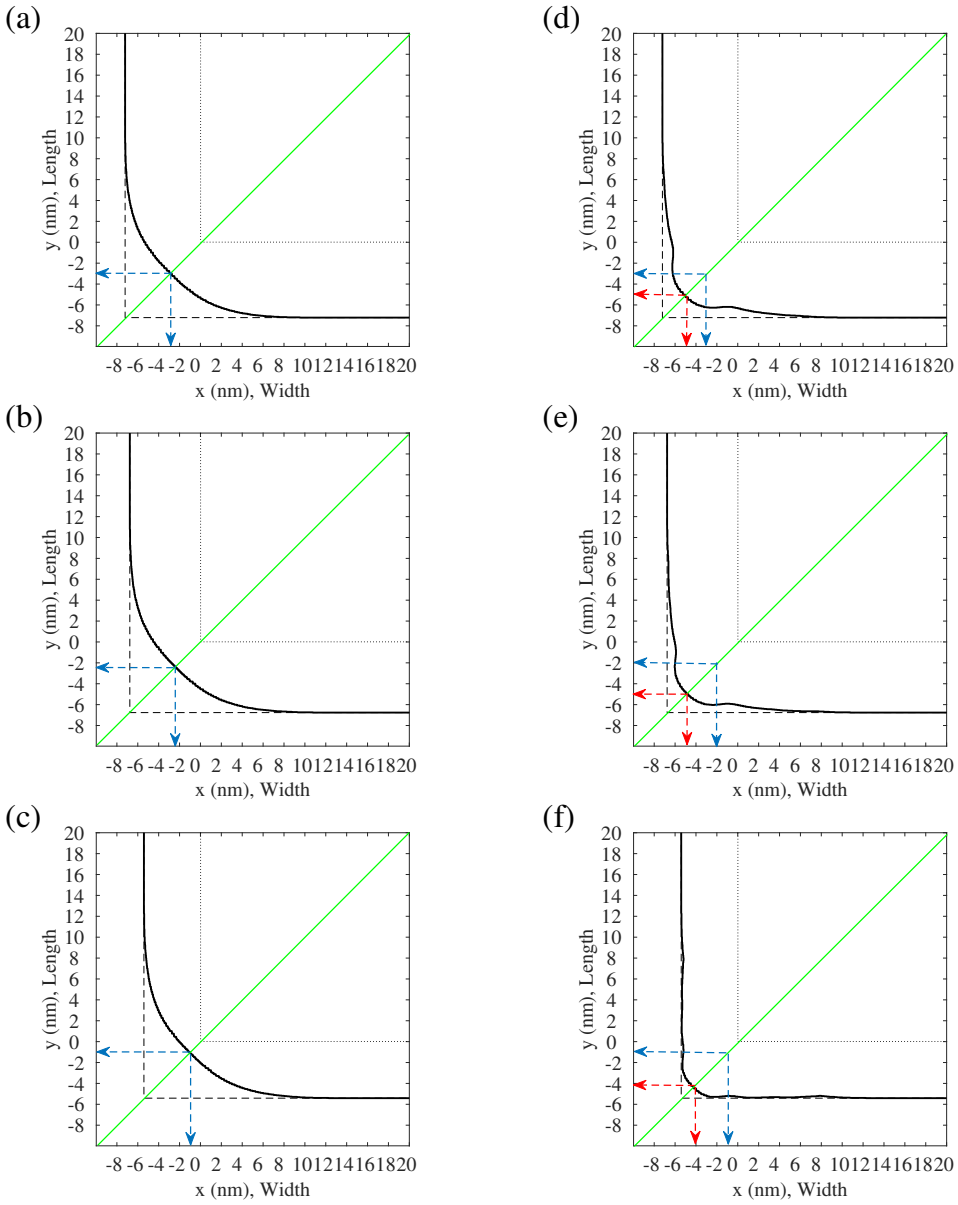

Figure 6.12: The development results before the correction at (a) top, (b) middle, and (c) bottom layer when σ = 4 nm. The two shots correction result at the (d) top, (e) middle, and (f) bottom layer. Each of the shots are a B_c = 2.5 nm square beam where the shot 1 is overlapped with a 1 nm x 1 nm square area with the regular beam exposed area. And the shot 2 is overlapped with a -2 nm x -2 nm square area with the regular beam exposed area. The shot 1 used a dose level of 1.3 and shot 2 used a dose level of 0.2 . $B = I_e$ = 10 nm and σ = 4 nm.

6.6 Correction Result after the Third Shot's Application

The third shot is chosen to overlap so that it would maximize directive development near the ideal corner of the top layer. Thus a minimum partial overlap with the developed area in respect to the middle layer as in Fig. 6.13 is chosen. The figure demonstrates the location of

2.5nm Square beam Gaussian (nm)	0.25 (nm)	0.5 (nm)	0.75 (nm)	1 (nm)
Amount of overlap between shot 1 and 2 (nm)	1.5nm	0.5nm	-0.5nm	-0.5nm

Table 6.4: The resulting amount of overlap between the shot 1 and shot 2 for the three shot correction using a 2.5 nm x 2.5 nm correction shot. $B = I_e = 10$ nm and $\sigma = 4$ nm.

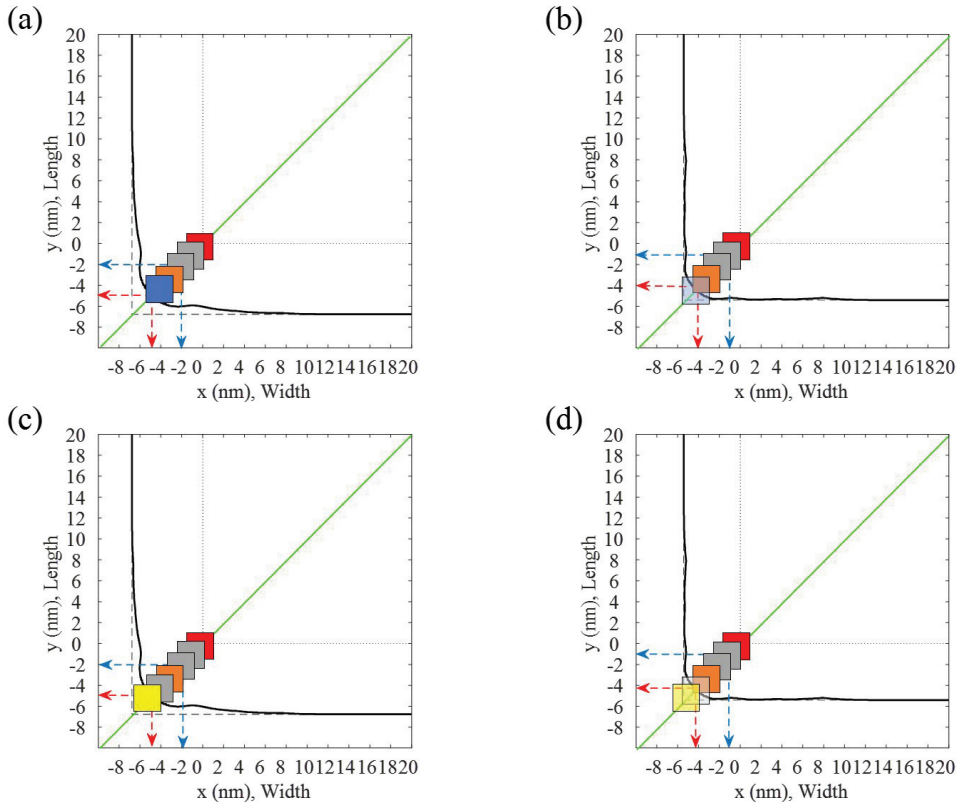

Figure 6.13: In this illustration, three correction shots are applied at the corner of the feature where the size is $B_c = 2.5$ nm square. The shot 1 is 1 nm x 1 nm overlapped (red square). The shot 2 is -2 nm x -2 nm overlapped (orange square). The shot 3 candidates are overlapped with a -3 nm x -3 nm square area (blue square) in (a) and (b) and -4 nm x -4 nm square area (yellow square) in (c) and (d) to the regular beam exposed area of the feature.

shot 3 in respect to the middle and bottom layer development after shot 2 is applied with an overlap of -3 nm in (a) and (b), and -4 nm in (c) and (d) from the corner of the regular beam exposed area. The squares are 2.5 nm x 2.5 nm sized correction shot which each of the corner of each squares are spaced in 1 nm apart. The red shots in (a-d) represent shot 1 with an overlap of 1 nm decided from the previous sections. The orange shots in (a-d) represent shot 2 with an overlap of -2 nm decided from the previous section. The blue shots in (a) and (b) represent

a candidate shot 3 with an overlap of -3 nm with the regular beam exposed area. The yellow shots in (c) and (d) represent a candidate shot 3 with an overlap of -4 nm with the regular beam exposed area. The gray shots in (a-d) are beams that are not exposed but included for illustrative purposes. The overlap amount refers to the amount between shot 3 and the regular corner shot of the feature, not between the shot 2 and shot 3.

Notice that although the overlap exceeds the bottom layer's ideal corner's position, a lower dose compared to shot 1 is used to target over the shallower layers as in Table 6.5(d). So, the bottom layer's development is minimal. The resulting correction is in Fig. 6.14. The correction is directive in that the x,y coordinates after the correction over the layers are consistently close to (x,y) = (-6 nm, -6 nm) as indicated by the red arrows from (d-f). If the simulation is allowed to overdevelop for the last correction shot for a directive correction at the top layer, the entire layer's % area reduction is at least 70% for the B = 10 nm and its simulated tf of σ = 1nm to 4nm as in Table 6.5(a-d). And the directivity over all layers are consistent as in Figs. 6.16, 6.17, 6.18, 6.19, 6.20, 6.21, and 6.22. For the 10 nm square beam with tf sharpness of σ = 1 nm, 2 nm, 3 nm, and 4 nm, the resulting choice of overlap amount of the shot 3 and the regular beam exposed area is -1 nm, -2 nm, -3 nm, and -4 nm, respectively as in Table 6.5. The overlap amount of the second shot and the third shot is 1.5nm, 1.5nm, 1.5nm, and 0.5nm for correction shot of sharpness 0.25nm, 0.5nm, 0.75nm and 1nm, respectively as in Table 6.6.

The dimension of a possible defect correction shape is smaller than the size of the correction shot. The width of the defect is larger as the blurring factor of the beam increases and is largest when B = 10 nm and *tf* of σ = 4 nm where the size is a little less than 1 nm as in the Fig. 6.14. If a more accurate correction pattern is required, a correction shot can be written along the feature side for the remaining areas. Then the correction result is as in Fig. 6.15 with two side shots at each side with a total of 4 side shots. The result produces a slight side stripe overdevelopment at the bottom layer as in Table 6.5(d) and Fig. 6.15(f) but, the overall correction directivity is kept consistent as in Fig. 6.15(d-f). From the simulation, placing two or more additional shots along each side of the feature in total of four shots produces a near perfect correction as seen in Fig. 6.16, 6.18, 6.20, and 6.22.

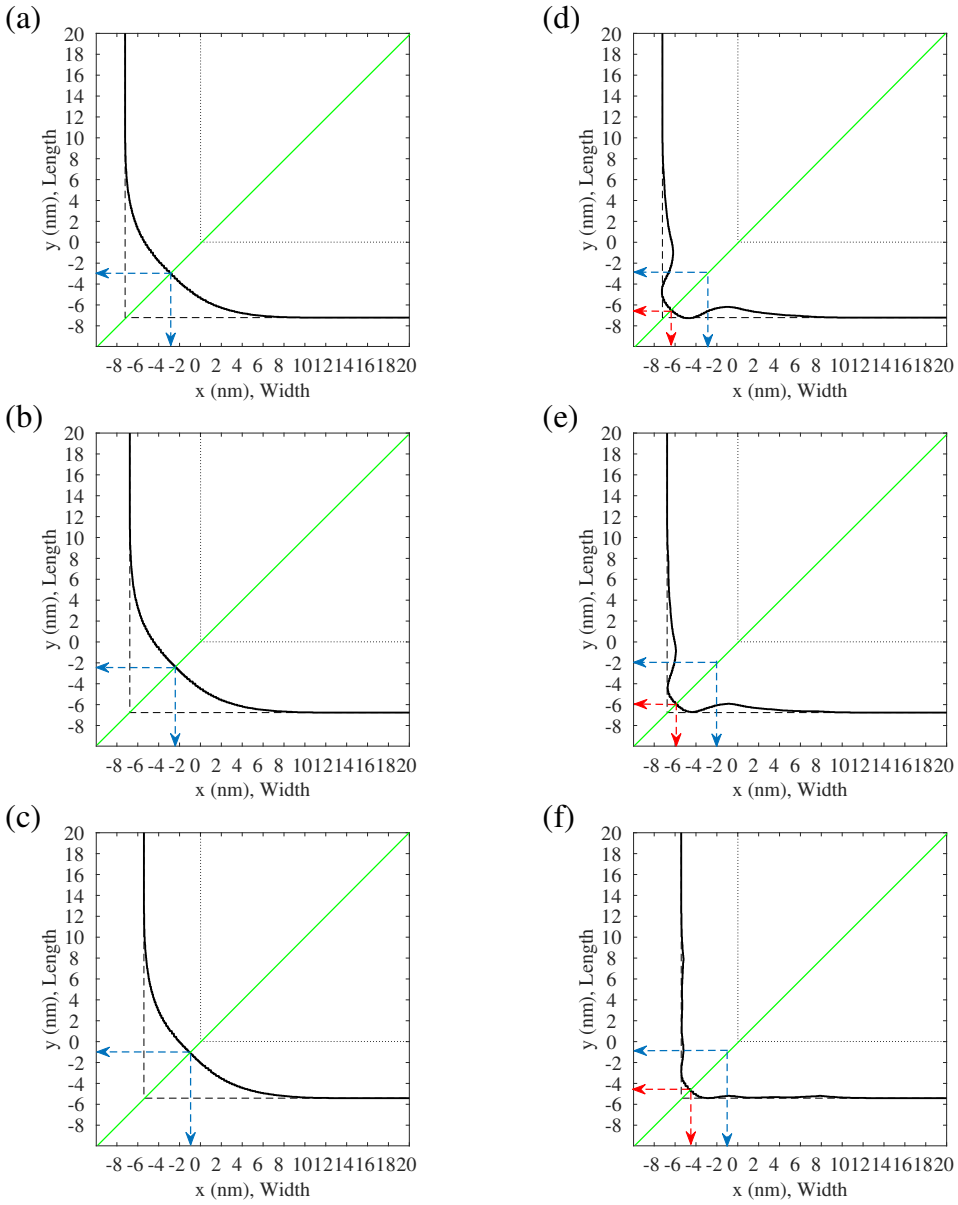

Figure 6.14: The development results before the correction at (a) top, (b) middle, and (c) bottom layer when σ = 4 nm. The three shots correction result at the (d) top, (e) middle, and (f) bottom layer. Each of the shots are a B_c = 2.5 nm square beam where the shot 1 is overlapped with a 1 nm x 1 nm square area, the shot 2 is overlapped with a -2 nm x -2 nm square area, and the shot 3 is overlapped with a -4 nm x -4 nm square area with the regular beam exposed area, respectively. The shot 1 used a dose level of 1.3, shot 2 used 0.2, and shot 3 used 0.16. $B = I_e$ = 10 nm and σ = 4 nm.

However, the correction from each additional shots are more expensive than each shot from the regular shots because both size shots can not be written at a same run. This is because the multi-beam system projects beams from the aperture plate having fixed uniform sizes and intervals of beams from one run. The use of smaller correction shots costs additional time to switch the projection system from the regular shot settings to correction shot settings. Also,

the additional correction shots are expensive because they need to be sequentially transferred. This is due to the fact that the three beam correction spaces have only 1 or 2 nm between the correction shots. The multi-beam transfers its beams synchronously in space of I_b. The beams that needs to be transferred less than the aperture's beam interval of I_b needs to be written at a different run. This results in longer correction time. The multi-beam system assumes the beam interval I_b is significantly larger than the beam size B and the areas between need to be addressed by all different beams which in this case all three beams and the side correction shots can not be transferred simultaneously. So, it is preferable to use as few correction shots as possible.

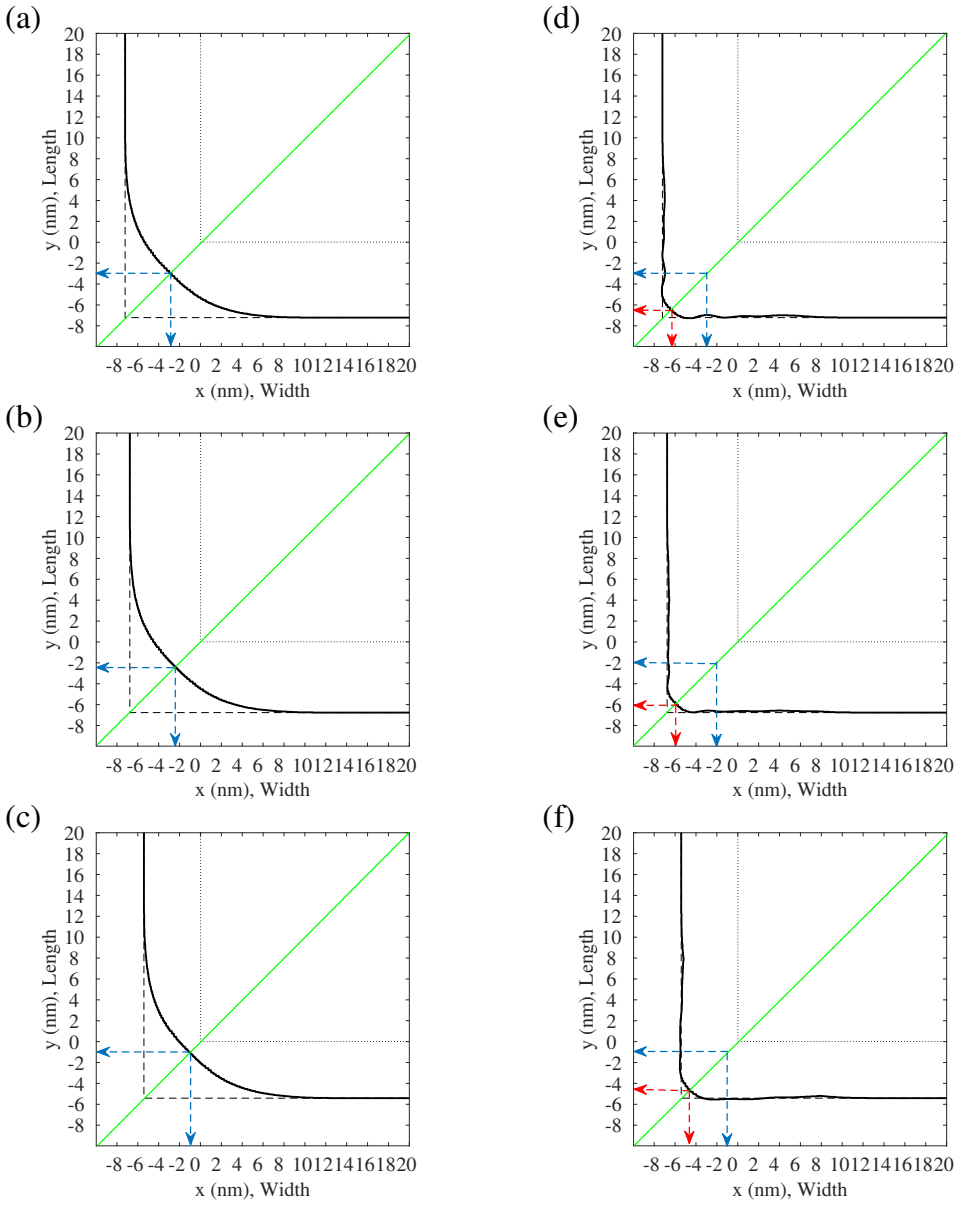

Figure 6.15: The three shots correction result at the (a) top, (b) middle, and (c) bottom layer when two side correction shots are additionally patterned at each edge of the feature. Each of the correction shots are a B_c = 2.5 nm square beam where the shot 1 is overlapped with a 1 nm x 1 nm square area, the shot 2 is overlapped with a -2 nm x -2 nm square area, and the shot 3 is overlapped with a -4 nm x -4 nm square area with the regular beam exposed area, respectively. The shot 1 used a dose level of 1.3, shot 2 used 0.2, and shot 3 used 0.16. The two side correction shots are spaced 8 nm apart along each feature side. The dose level used are each 0.05 and 0.02. $B = I_e$ = 10 nm and σ = 4 nm.

6.7 Faulty Beam

One of the factors determining how a faulty beam affects the writing quality is the location of the point exposed by the faulty beam. The effect would be larger when the point is closer to the feature boundary. Also, the effect of a faulty beam may vary significantly depending on the writing redundancy and exposing interval. The writing redundancy refers to the number of beams jointly exposing a point,[7,8] e.g., 2-beam redundancy corresponds to the case where each point is exposed by 2 different beams. In Table 6.7 and Fig. 6.23, the LER and maximum indent are provided for the cases of one faulty beam. It is first observed that a faulty beam can affect the writing quality substantially, especially when an edge point is exposed by the faulty beam. When a point in the middle of a feature receives a lower exposure due to a faulty beam, the isotropic development of resist can mitigate the effect of lower exposure on the final feature boundary through the developing process. However, in the case of a lower exposure of an edge point, such mitigation would be minimal since the edge points are developed in the final stage of resist development. Also, it is seen that the effects on the LER and maximum indent are larger for a higher writing redundancy and a smaller exposing interval. This is due to the fact that the exposure drop due to a faulty beam is smaller when a point is exposed by a larger number of beams (i.e., a higher writing redundancy) or the exposing interval is smaller leading to a larger overlap between the domains of two adjacent beams on the resist surface.

In Fig. 6.24, the contours of remaining resist profile are shown with the writing redundancy varied. It can be seen that the boundary roughness, in particular the maximum indent, is larger for a smaller writing redundancy and the effect of a faulty beam is maximized when it exposes edge points (see Fig. 6.24-(b)).

Added beam	Overlap (nm)	Dose	Top		Middle		Bottom	
			% area reduced	Over developed area (nm)	% area reduced	Over developed area (nm)	% area reduced	Over developed area (nm)
Shot 1	1	0.13	-49.77	0	-56.01	0	-69.19	0.011
Shot 2	0	0.01	-77.48	0.017	-74.92	0	-75.93	0.011
Shot 3	-1	0.01	-89.53	0.102	-83.16	0	-77.82	0.011

(a)

Added beam	Overlap (nm)	Dose	Top		Middle		Bottom	
			% area reduced	Over developed area (nm)	% area reduced	Over developed area (nm)	% area reduced	Over developed area (nm)
Shot 1	1	0.8	-29.85	0	-41.43	0	-69.30	0
Shot 2	-1	0.05	-63.77	0	-68.64	0	-84.05	0
Shot 3	-2	0.02	-74.13	0	-75.79	0	-86.63	0
Side shots	side		-83.54	0	-86.00	0	-90.18	0.352

(b)

Added beam	Overlap (nm)	Dose	Top		Middle		Bottom	
			% area reduced	Over developed area (nm)	% area reduced	Over developed area (nm)	% area reduced	Over developed area (nm)
Shot 1	1	1	-28.14	0	-40.40	0	-72.12	0
Shot 2	-2	0.14	-65.08	0	-70.87	0	-89.29	0
Shot 3	-3	0.04	-72.92	0	-76.62	0	-91.22	0.012
Side shots	side		-90.31	0.222	-88.69	0.136	-94.85	0.204

(c)

Added beam	Overlap (nm)	Dose	Top		Middle		Bottom	
			% area reduced	Over developed area (nm)	% area reduced	Over developed area (nm)	% area reduced	Over developed area (nm)
Shot 1	1	1.3	-29.32	0	-42.34	0	-71.90	0
Shot 2	-2	0.2	-51.86	0	-62.91	0	-87.47	0
Shot 3	-4	0.16	-71.19	0.034	-75.96	0	-90.47	0
Side shots	side		-89.47	0.04	-88.95	0	-93.24	0.457

(d)

Table 6.5: The cumulative correction result after each shot is patterned for a three shots correction. Each shot's choice of amount of overlap, dose level, and the corresponding correction results at top, middle, and bottom layers is presented. $B = I_e = 10$ nm and tf of the correction shot is of σ = (a) 0.25, (b) 0.5, (c) 0.75, and (d) 1 nm.

2.5nm Square beam Gaussian (nm)	0.25 (nm)	0.5 (nm)	0.75 (nm)	1 (nm)
Amount of overlap between shot 1 and 2 (nm)	1.5nm	1.5nm	1.5nm	0.5nm

Table 6.6: The resulting amount of overlap between the shot 2 and shot 3 for the three shot correction using a 2.5 nm x 2.5 nm correction shot. B = I_e = 10 nm and σ = 4 nm.

I_e (nm)	LER (nm)				Maximum indent (nm)			
	no fault	Redundancy			no fault	Redundancy		
		1	2	4		1	2	4
1	0	0	0	0	0	0	0	0
2	0.020	0.028	0.023	0.019	0.029	0.052	0.039	0.031
5	0.18	0.21	0.19	0.19	0.29	0.43	0.36	0.34
10	0.34	0.41	0.39	0.39	0.72	1.06	1.12	1.14

(a)

I_e (nm)	LER (nm)				Maximum indent (nm)			
	no fault	Redundancy			no fault	Redundancy		
		1	2	4		1	2	4
1	0	0	0	0	0	0	0	0
2	0.020	0.041	0.026	0.021	0.029	0.082	0.047	0.037
5	0.18	0.69	0.43	0.30	0.29	1.05	0.86	0.61
10	0.34	2.02	1.86	1.24	0.72	4.16	3.58	3.47

(b)

Table 6.7: The LER and maximum indent with the redundancy varied for the line-width (W) of 50 nm (a) when the faulty beam exposes points in the middle of feature and (b) when the faulty beam exposes points on the feature boundary: I_e = 10 nm and σ = 2 nm. The LER and maximum indent when no beam is faulty are also included for reference.

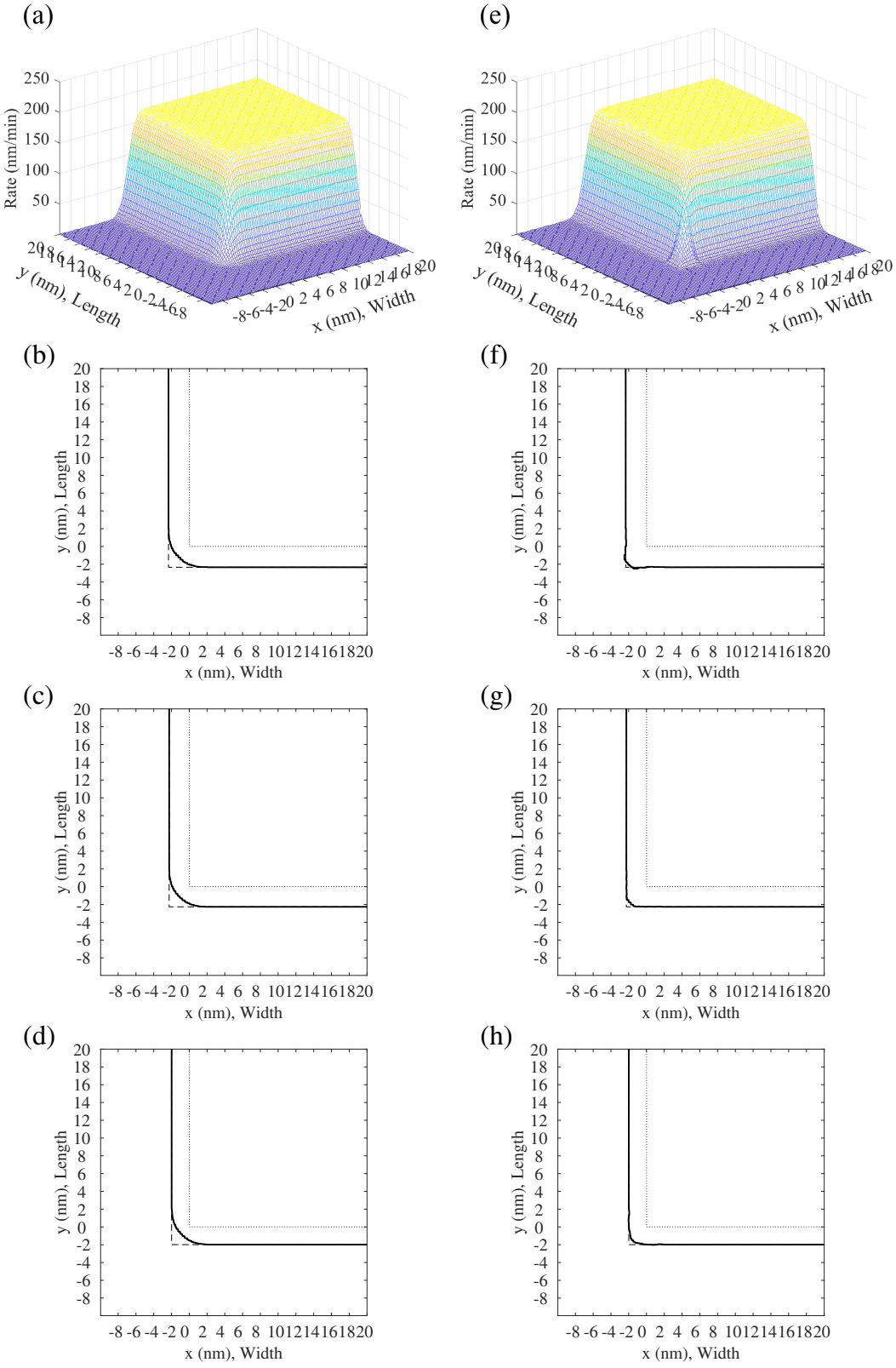

Figure 6.16: The results of before and after the correction using a B_c = 2.5 nm square beam is presented where the shot 1, shot 2, and shot 3 are overlapped with 1 nm x 1 nm, 0 nm x 0 nm , and 1 nm x 1 nm square area with the regular beam exposed area, respectively. The shot 1, shot 2, and shot 3 used a dose level of 0.13, 0.01, and 0.01, respectively. The rate plots of the middle layer at the feature corner is shown in (a) before and after (e). The development results of top layer are presented in (b) before and (f) after, middle layer in (c) before and (g) after, and bottom layer in (d) before and (h) after. $B = I_e$ = 10 nm and σ = 1 nm.

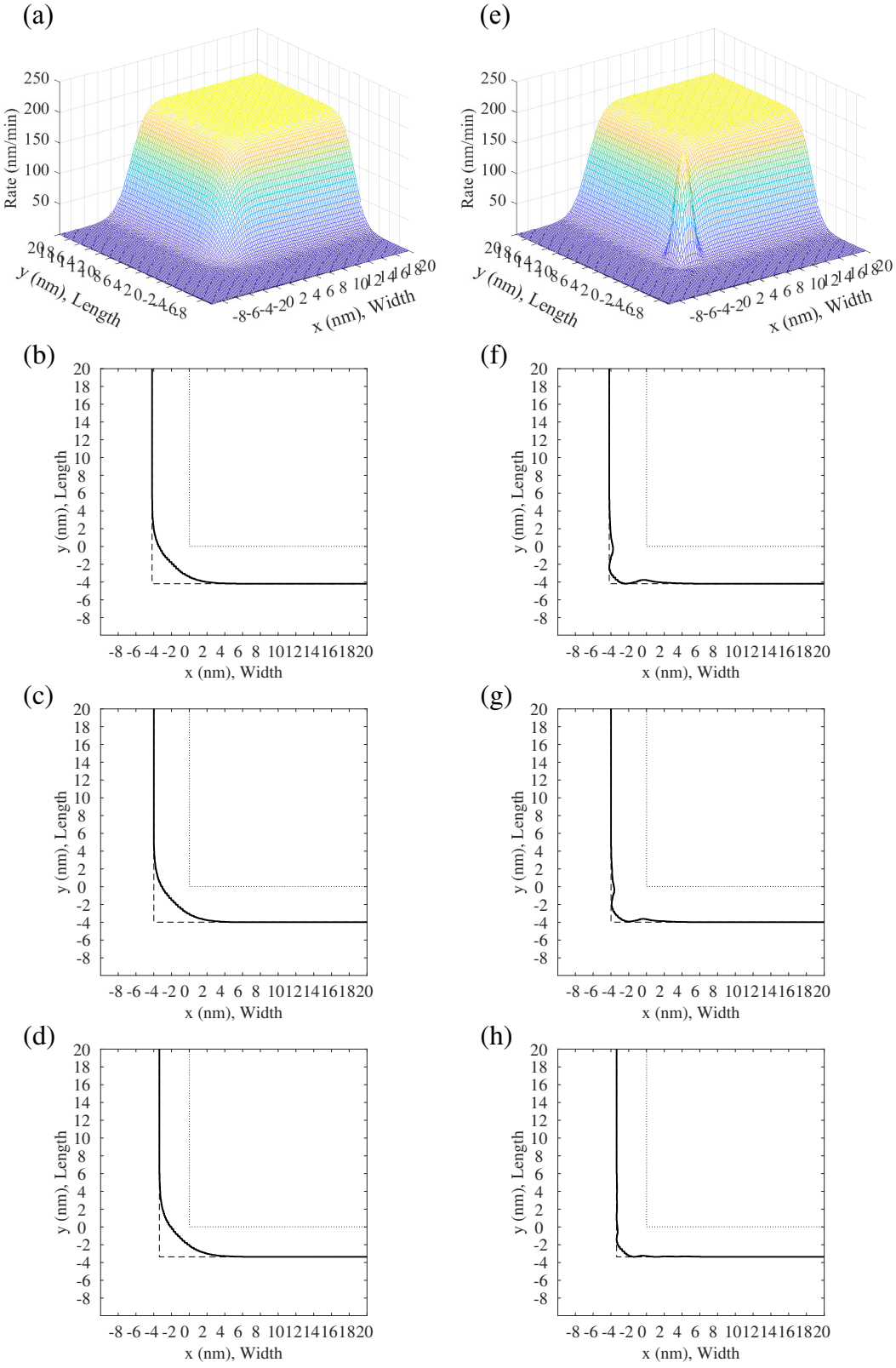

Figure 6.17: The results of before and after the correction using a B_e = 2.5 nm square beam where the shot 1, shot 2, and shot 3 are overlapped with a 1 nm x 1 nm, -1 nm x -1 nm, and -2 nm x -2 nm square area with the regular beam exposed area, respectively. The shot 1, shot 2, and shot 3 used a dose level of 0.8, 0.05, and 0.02, respectively. The rate plots of the middle layer at the feature corner is shown in (a) before and after (e). The development results of top layer are presented in (b) before and (f) after, middle layer in (c) before and (g) after, and bottom layer in (d) before and (h) after. $B = I_e$ = 10 nm and σ = 2 nm.

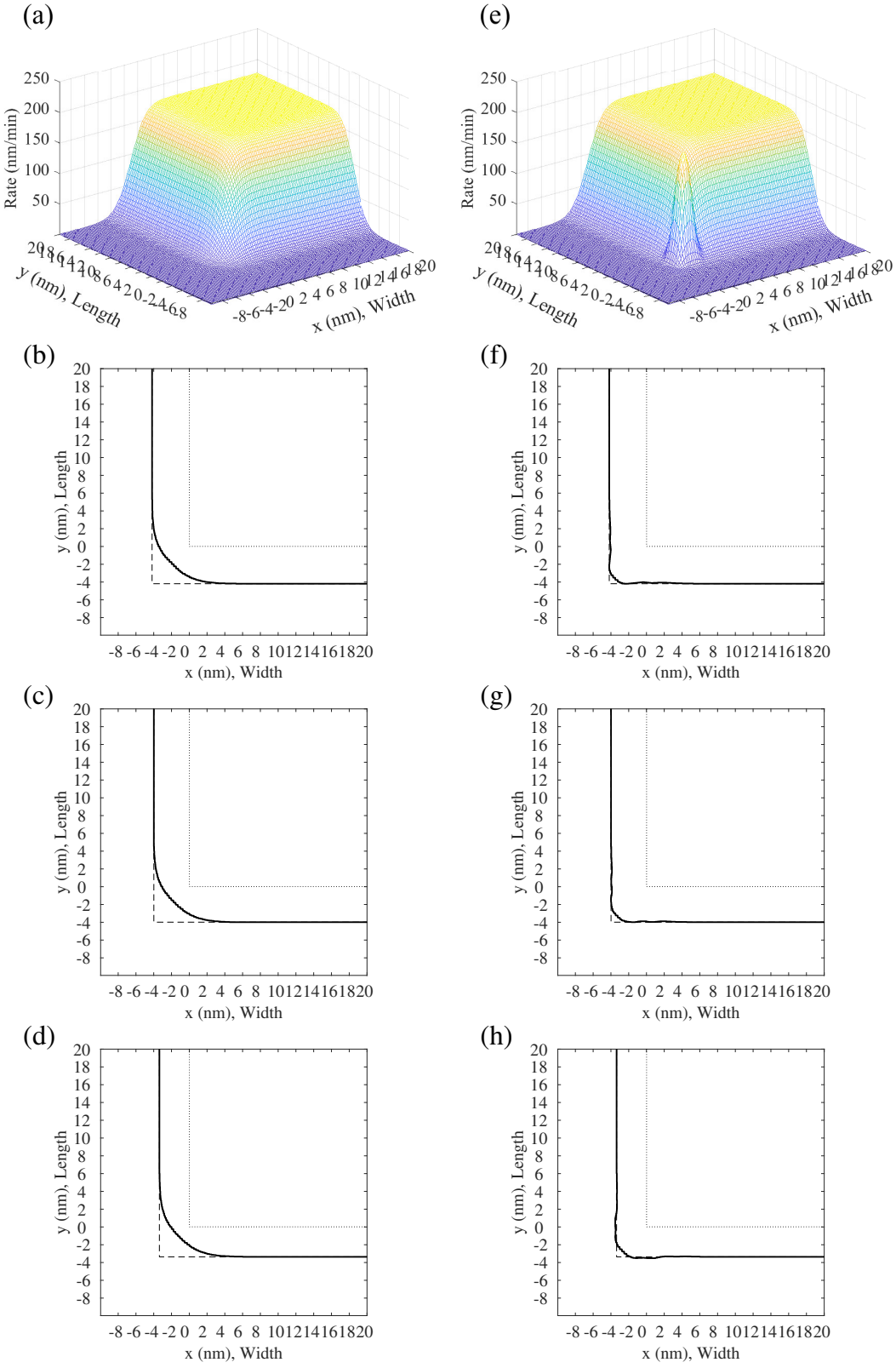

Figure 6.18: The results of before and after the correction using a B_c = 2.5 nm square beam where the shot 1, shot 2, and shot 3 are overlapped with a 1 nm x 1 nm, -1 nm x -1 nm, and -2 nm x -2 nm square area with the regular beam exposed area, respectively. The one side correction shot is patterned along each feature side. The dose level used is 0.02. The shot 1, shot 2, and shot 3 used a dose level of 0.8, 0.05, and 0.02, respectively. The rate plots of the middle layer at the feature corner is shown in (a) before and after (e). The development results of top layer are presented in (b) before and (f) after, middle layer in (c) before and (g) after, and bottom layer in (d) before and (h) after. $B = I_e$ = 10 nm and σ = 2 nm.

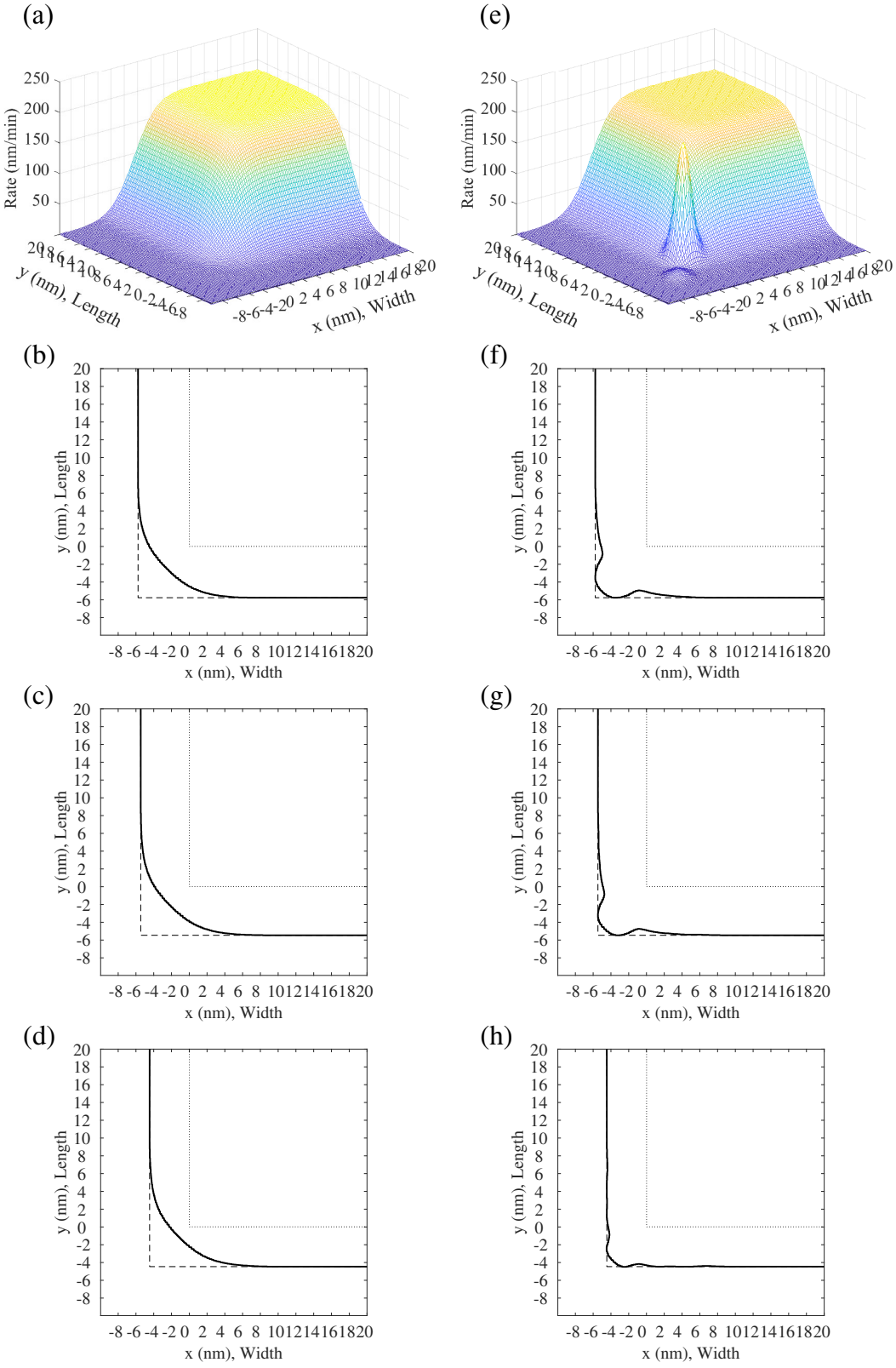

Figure 6.19: The results of before and after the correction using a B_c = 2.5 nm square beam where the shot 1, shot 2, and shot 3 are overlapped with a 1 nm x 1 nm, -2 nm x -2 nm, and -3 nm x -3 nm square area with the regular beam exposed area, respectively. The shot 1, shot 2, and shot 3 used a dose level of 1, 0.14, and 0.04, respectively. The rate plots of the middle layer at the feature corner is shown in (a) before and after (e). The development results of top layer are presented in (b) before and (f) after, middle layer in (c) before and (g) after, and bottom layer in (d) before and (h) after. $B = I_e$ = 10 nm and σ = 3 nm.

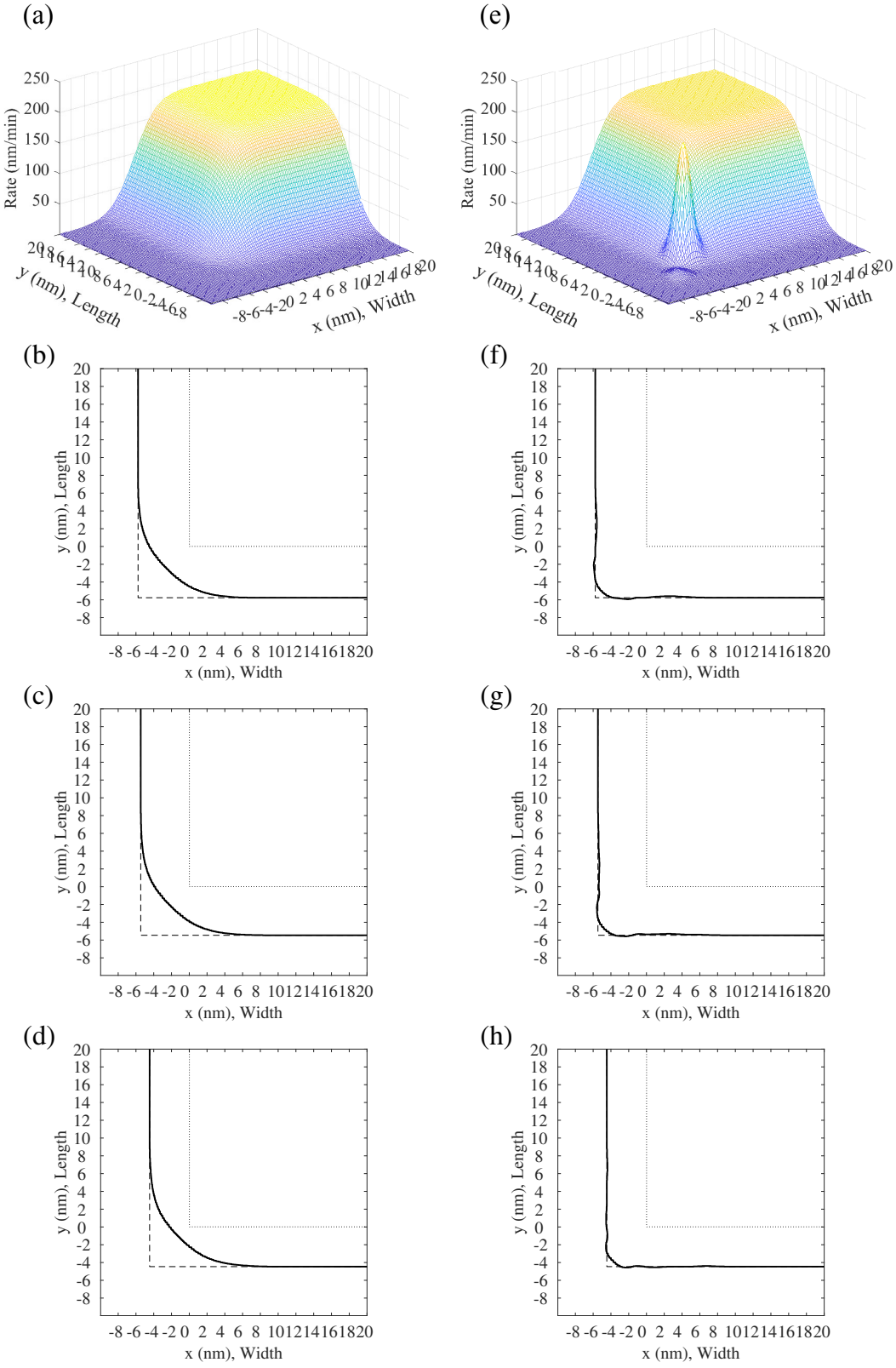

Figure 6.20: The results of before and after the correction using a B_e = 2.5 nm square beam where the shot 1, shot 2, and shot 3 are overlapped with a 1 nm x 1 nm, -2 nm x -2 nm, and -3 nm x -3 nm square area with the regular beam exposed area, respectively. The shot 1, shot 2, and shot 3 used a dose level of 1, 0.14, and 0.04, respectively. The two side correction shots are spaced 8 nm apart along each feature side. The dose level used are each 0.01 and 0.03. The rate plots of the middle layer at the feature corner is shown in (a) before and after (e). The development results of top layer are presented in (b) before and (f) after, middle layer in (c) before and (g) after, and bottom layer in (d) before and (h) after. $B = I_e$ = 10 nm and σ = 3 nm.

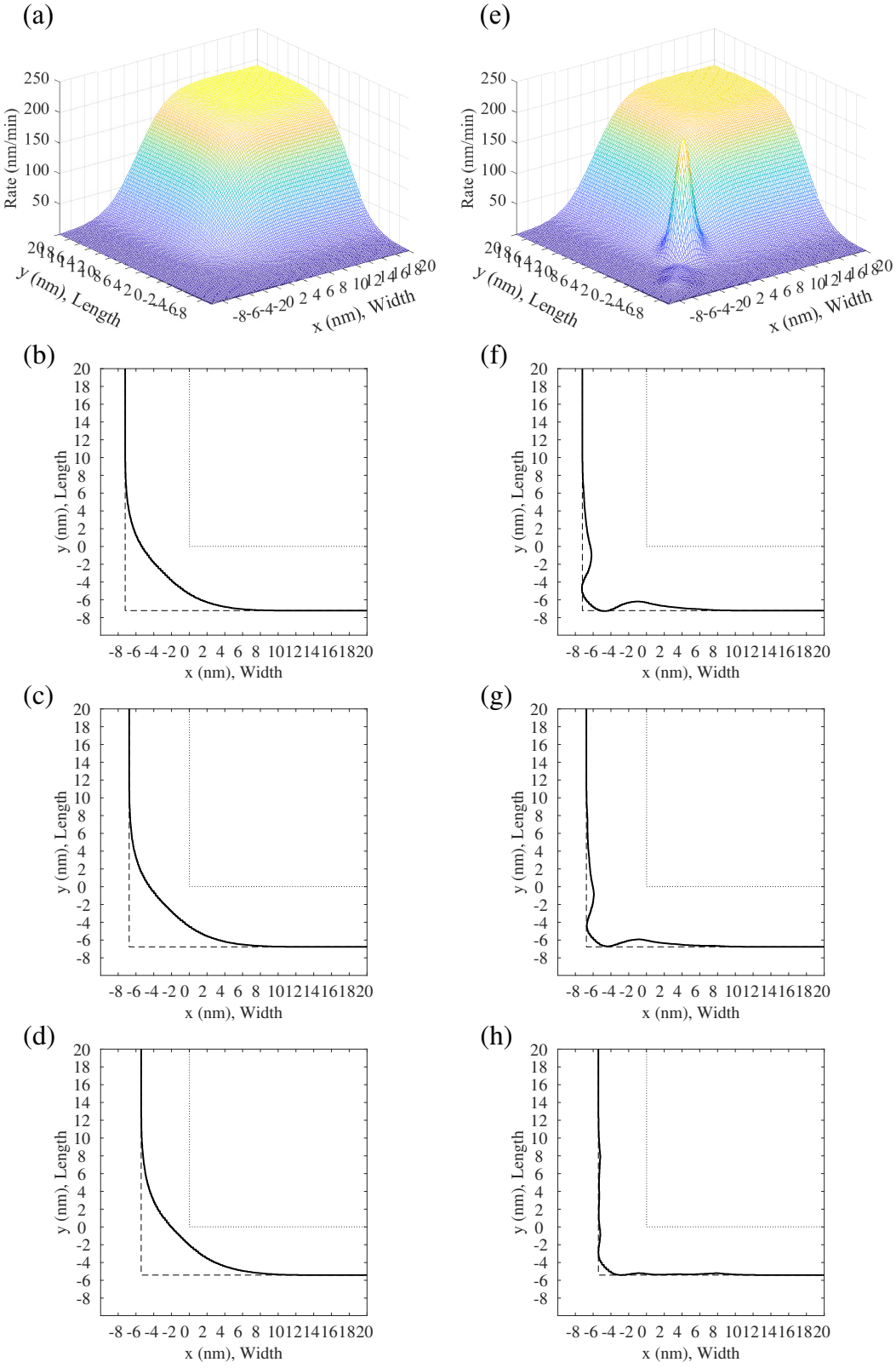

Figure 6.21: The results of before and after the correction using a B_c = 2.5 nm square beam where the shot 1, shot 2, and shot 3 are overlapped with a 1 nm x 1 nm, -2 nm x -2 nm, and -4 nm x -4 nm square area with the regular beam exposed area, respectively. The shot 1, shot 2, and shot 3 used a dose level of 1.3, 0.2, and 0.16, respectively. The rate plots of the middle layer at the feature corner is shown in (a) before and after (e). The development results of top layer are presented in (b) before and (f) after, middle layer in (c) before and (g) after, and bottom layer in (d) before and (h) after. B = I_e = 10 nm and σ = 4 nm.

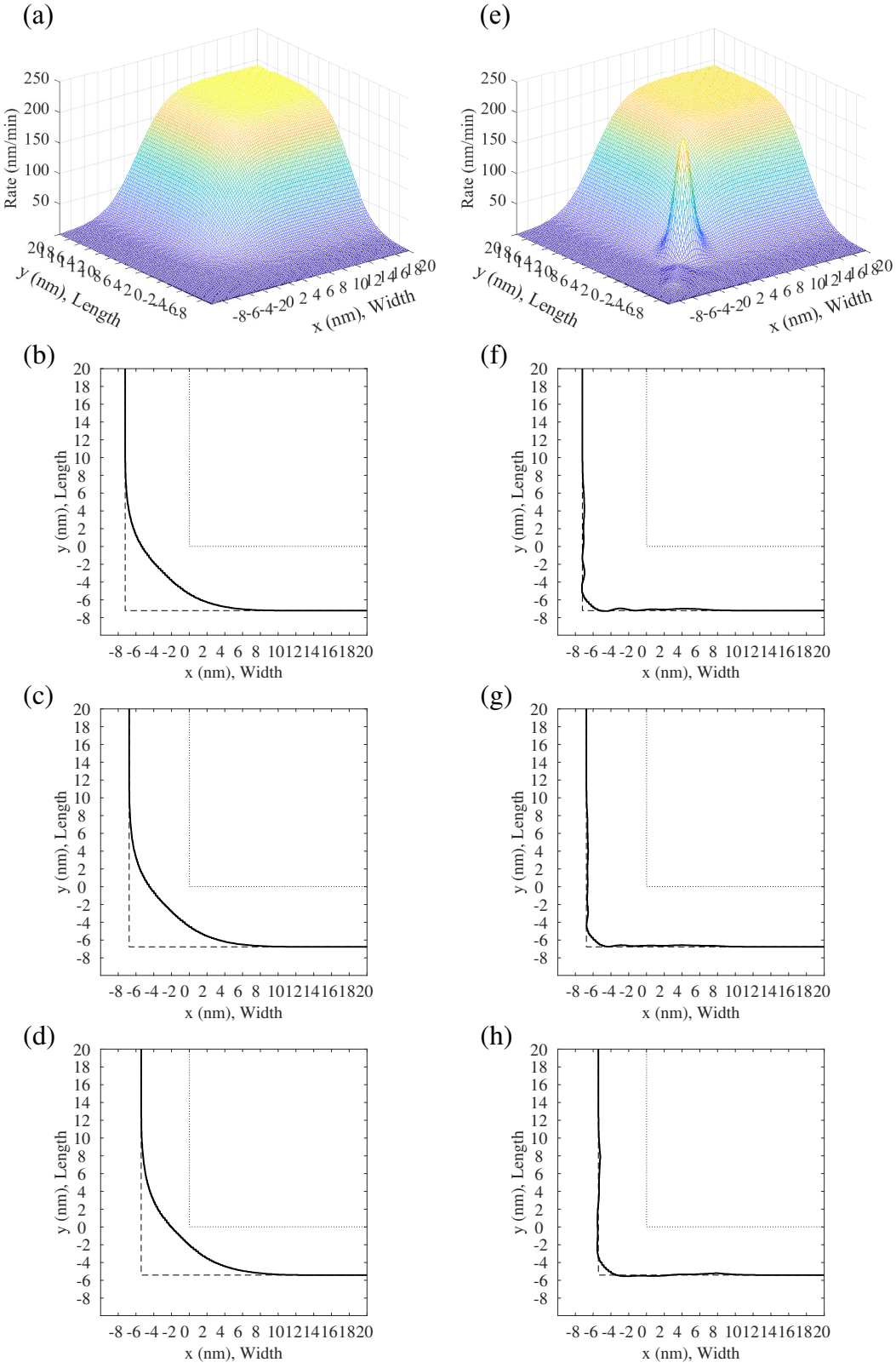

Figure 6.22: The results of before and after the correction using a B_e = 2.5 nm square beam where the shot 1, shot 2, and shot 3 are overlapped with a 1 nm x 1 nm, -2 nm x -2 nm, and -4 nm x -4 nm square area with the regular beam exposed area, respectively. The shot 1, shot 2, and shot 3 used a dose level of 1.3, 0.2, and 0.16, respectively. The two side correction shots are spaced 8 nm apart along each feature side. The dose level used are each 0.02 and 0.05. The rate plots of the middle layer at the feature corner is shown in (a) before and after (e). The development results of top layer are presented in (b) before and (f) after, middle layer in (c) before and (g) after, and bottom layer in (d) before and (h) after. $B = I_e$ = 10 nm and σ = 4 nm.

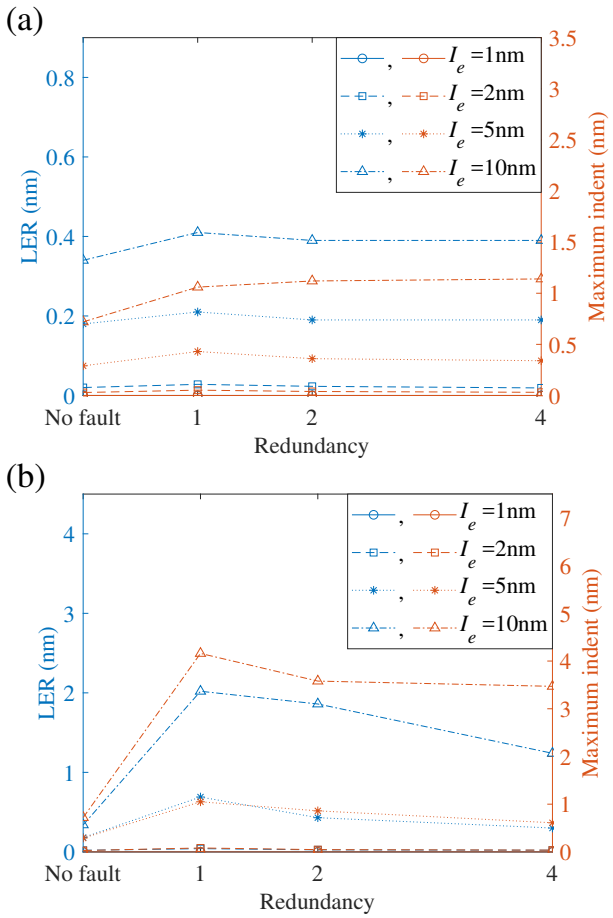

Figure 6.23: The LER and maximum indent in nm with the redundancy varied for the line-width (W) of 50 nm (a) when the faulty beam exposes points in the middle of feature and (b) when the faulty beam exposes points on the feature boundary: I_e = 10 nm and σ = 2 nm. The LER and maximum indent when no beam is faulty are also included for reference.

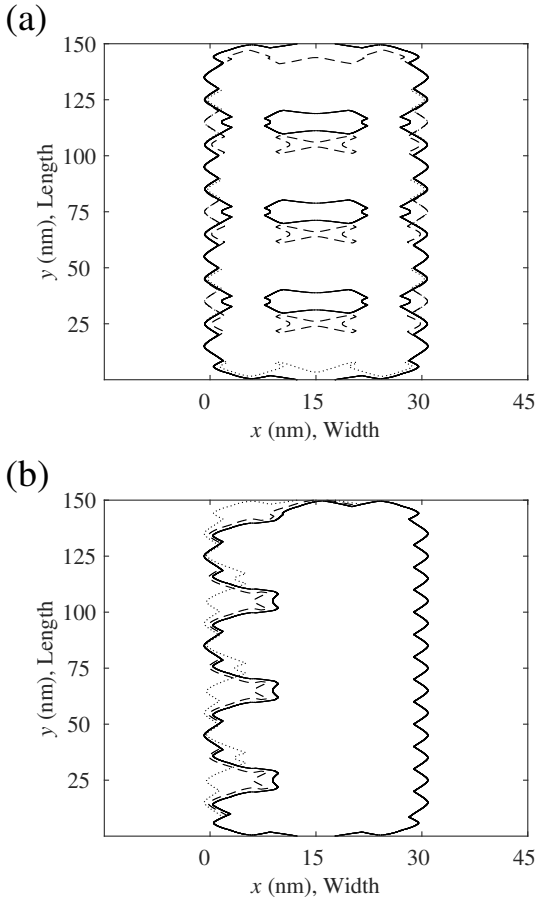

Figure 6.24: The contour of remaining resist profile for the line-width (W) of 30 nm: (a) when center points are exposed by a faulty beam and (b) left edge points are exposed by a faulty beam. It is assumed that a point receives no dose from a faulty beam. B = I_e = 10 nm and σ = 4 nm. The contours for the 1-beam, 2-beam and 4-beam redundancies are indicated by the red, green and blue curves, respectively.

Chapter 7

Summary

The inherent drawback of an e-beam lithography system has been its low throughput due to the use of a single beam. The main effort to improve the throughput by orders of magnitude has been to employ multiple beams in a system. As a result, e-beam systems with massively-parallel beams were recently developed. To maximize the efficiency of such a system, it is critical to utilize the parallel beams in an optimal way. As a first step, this study investigates the effects of the lithographic parameters on the writing qualities. And subsequently explores the beam exposure methods and controls to improve the proximity effect on the pattern corner for the mask production. The lithographic parameters such as the exposing interval, blurring factor, writing redundancy, etc. are considered, and the quality metrics including the exposure variation and contrast, total dose required, dose latitude, line edge roughness, corner rounding, and directivity are analyzed. This study corrects the rounded corner of the feature by serially patterning a shot that is $\frac{1}{4}$ of the regular shot from outside of the beam exposed area toward the ideal corner of the feature. Each exposure contributes a slightly different electron beam path for different depths that is designed to sharpen near the mask's corners evenly throughout the depth in cumulative shots. Through an extensive simulation, it is seen that the proposed method possibly results in a non-unique solution having a range of working combinations of position and dose for each beam that produces similar results. The proposed strategy is able to produce a directive correction for a pattern that results in having a width development difference over the depth without correction. Applying side shots at the pattern is found to complement the proposed strategy. Though the quantitative results may vary depending on the simulation set-up, the behaviors of the correction method are likely to be similar with those reported in this paper. This study presented effective guidelines for the design decision of each correction shot

for optimal use of a massively-parallel e-beam system. Based on the simulation, the correction shots are expensive both from the amount of shot interval necessary and the shot size switching time of the massively-parallel e-beam system such that the proximity correction can not be done simultaneously with the regular feature patterning process.

ACKNOWLEDGEMENT

This work was supported in part by a research grant from Samsung Electronics Co., Ltd.

References

[1] S.-Y. Lee and B. D. Cook, IEEE Trans. Semicond. Manuf. **11**, 117 (1998).

[2] U. Hofmann, R. Crandall, and L. Johnson, J. Vas. Sci. Technol. B **17**, 2940 (1999).

[3] M. Osawa, K. Takahashi, M. Sato, H. Arimoto, K. Ogino, H. Hoshino, and Y. Machida, J. Vac. Sci. Technol. B **19**, 2483 (2001).

[4] S.-Y. Lee, S.C. Jeon, J.S. Kim, K.N. Kim, M.S. Hyun, J.J. Yoo, and J.W. Kim, J. Vac. Sci. Technol., B **27**, 2580 (2009).

[5] Q. Dai, S.-Y. Lee, S.-H. Lee, B.-G. Kim, and H.-K. Cho, J. Vac. Sci. Technol. B **30**, 06F307 (2012).

[6] C. Klein, H. Loeschner, and E. Platzgummer, J. Micro/Nanolithogr. MEMS MOEMS. **11**, 031402 (2012).

[7] H. Fragner and E. Platzgummer, U.S. Patent 7777201 B2 (17 August 2010).

[8] H. Fragner, E. Platzgummer, R. Nowak, and A. Bürli, U.S. Patent 8222621 B2 (17 July 2012).

[9] H. Matsumoto, H. Inoue, H. Yamashita, H. Morita, S. Hirose, M. Ogasawara, H. Yamada, and K. Hattori, Hattori, Proc. SPIE **9984**, 998405 (2016).

[10] P. Petric, C. Bevis, A. Carroll, H. Percy, M. Zywno, K. Standiford, A. Brodie, N. Bareket, and L. Grella, J. Vac. Sci. Technol. B **27**, 161 (2009).

[11] T. Kamikubo, K. Ohtoshi, S. Golladay. V. Katsap, R. Kendall, H. Sunaoshi, and S. Tamamushi, Phys Procedia, **1**, 119 (2008).

[12] M. A. Hanapiah, Y.-K. Sin, and K. Ibrahim, AIP Conf. Proc., **1017**, 99 (2008).

[13] C. Tang, M. Su, and Y. Lu, J. Micro/Nanolithogr. MEMS MOEMS **14**, 031212 (2015).

[14] C.-C. Fu, T. Yang, and D.R. Stone, IEEE Trans. Electron Devices, **38**, 2599-2603 (1991).

[15] S.-Y. Lee, F. Hu, and J. Ji, J. Vac. Sci. Technol. B **22**, 2929 (2004).

[16] C. S. Ea and A. D. Brown, J. Vac. Sci. Technol. B **19**, 1985 (2001).

[17] A. Starikov, Proc. SPIE **1088** (1989).

[18] J. F. Chen, U.S. Patent 5707765A (13 January 1998).

[19] Z. Huang, L. Ni, K. Fujii, and X. Huang, Proc. SPIE **11148**, 1114813 (2019).

[20] M. Mukherjee, V. Phan, Proc. SPIE **4691** (2002).

[21] K. -H. Choi, C. Browning, T. Figueiro, C. Hohle, M. Kaiser, and P. Schiavone, Proc. SPIE **9235**, 92350U (2014).

[22] H. Liu, S. F. Schulze, A. C. Thomas, A. E. McGuire, and M. Cross, Proc. SPIE **4181** (2000).

[23] E. Platzgummer, C. Klein, H. Loeschner, C. Hohle, M. Kaiser, and P. Schiavone, J. Micro/Nanolithgr. MEMS MOEMS **12**, 031108 (2013).

[24] Q. Dai, R. Guo, S.-Y. Lee, J. Choi, S.-H. Lee, I.-K. Shin, and C.-U. Jeon, Microelectron. Eng., **127**, 86 (2014).

[25] S. Johnson, Simulation of electron scattering in complex nanostructures: Lithography, metrology and characterization, Ph.D. dissertation (Cornell University, 1992).

[26] G. Lerondel, S. Kostcheev, and J. Plain, Nanofabrication for Plasmonics, Springer Series in Optical Sciences, 279, (2012)

[27] L. Ren and B. Chen, Proc. 7th Int. Conf. on Solid-State and Integrated Circuits Technology, **1**, 579-582 (2004).

[28] T. H. P. Chang, J. Vac. Sci. Technol. **12**, 1271 (1975).

[29] S. J. Wind, M. G. Rosenfield, G. Pepper, W. W. Molzen, and P. D. Gerber, J. Vac. Sci. Technol. B **7**, 1507 (1989).

[30] B. Dal'zotto, H. Dugourd, M. Lerme, and F. Meot, Microelectron. Eng., **3**, 105-110 (1985).